



Modelling and Control of PMSG Based Offshore Wind Turbine

Joan Francesc Quetglas Villalonga

Thesis to obtain the Master of Science Degree in
Energy Engineering and Management

Supervisors: Prof. Rui Manuel Gameiro de Castro
Prof. Oriol Gomis-Bellmut

Examination Committee

Chairperson: Prof. Duarte de Mesquita e Sousa

Supervisor: Prof. Rui Manuel Gameiro de Castro

Member of the Committee: Prof. Sónia Maria Nunes dos Santos Paulo Ferreira Pinto

September 2022

Declaration

I declare that this document is an original work of my own authorship and that it fulfills all the requirements of the Code of Conduct and Good Practices of the Universidade de Lisboa.

Abstract

O objetivo deste projeto é modelar uma turbina eólica que aciona um gerador síncrono de magnetos permanentes (PMSG) e projetar o sistema de controle capaz de suportar e recuperar cavas de tensão. Além disso, este projeto demonstra a eficiência do conversor de fonte de tensão (VSC) na mitigação dos efeitos das cavas de tensão na estabilidade da rede. O conversor do lado do gerador ajusta o gerador síncrono e desacopla-o da rede quando necessário, por exemplo, quando ocorrem cavas de tensão.

Por outro lado, o conversor do lado da rede supervisiona o fluxo de energia entre o barramento CC e o lado CA. Além disso, o modelo de Fault Ride Through evidencia a capacidade de recuperação rápida após a eliminação de um defeito. Os resultados da simulação no Matlab Simulink 2021b mostram que o modelo apresenta uma boa resposta dinâmica possibilitando a rápida recuperação após uma cava de tensão, estabilizando a turbina.

The aim of this project is to model a wind turbine driven by permanent magnetic synchronous generator (PMSG) and to design the control of the WT able to support and recover from voltage sags. Moreover, this project demonstrates the efficiency and the effects of a voltage sag on the grid stability and the robustness of the voltage source converter (VSC) as converter in the WT world.

The generator side inverter, adjusts the synchronous generator and decouples it from the grid when necessary, for example when the voltage sags occurs. On the other hand, the grid-side inverter oversees the power flow between the DC bus and the AC side. Moreover the fault-ride through capability has the capability to recover fast after a fault clearance. The simulation results in Matlab Simulink 2021b shows that the model has good dynamics and it recovers with a short time after a voltage drop, stabilizing the turbine.

Keywords

Conversor de fonte de tensão, passagem de falha, energia eólica, PMSG

Voltage Source Converter, Fault Ride Through, Wind Power, PMSG

Acknowledgments

First of all, I would like to express my gratitude to supervisor Dr. Rui Castro, Associate Professor at the Power Systems Section, Electrical and Computer Engineering Department of Técnico Lisboa (IST) and researcher at INESC-ID/IST, for granting for opportunity to write my master thesis in IST under his supervision even being working remotely.

Next, I would like to express my thanks to Dr. Oriol Gomis-Bellmunt, professor in the department of Electrical Engineering of Universitat Politècnica de Catalunya (UPC), and researcher in CITCEA, who allowed me to be guided the master thesis at the research center.

Above all, I would like to give my highest thanks to Dr. Jie Song, Project Engineer at CITCEA, who has guided me on this thesis even remotely. He has dedicated his best to guide the thesis, providing materials and knowledge from the start to the end.

Contents

- 1 CHAPTER 1: Introduction** **9**

 - 1.1 Background 11
 - 1.1.1 Problem Statement 11
 - 1.1.2 Aims and Objectives 11
 - 1.1.3 Thesis methodology 12
 - 1.1.4 Thesis outline 12

- 2 CHAPTER 2: Literature Review of Fault Ride-Through** **13**

 - 2.1 Series Dynamic Braking Resistor (SDBR) strategy 16
 - 2.2 Capacitive Bridge Fault Current Limiter (CBFCL) strategy 18
 - 2.3 Bridge Fault Current Limiter (BFCL) strategy 20

- 3 CHAPTER 3: Modelling and control - Type 4 turbine** **23**

 - 3.1 Wind turbine modelling 24
 - 3.1.1 Aerodynamics modelling 24
 - 3.2 PMSG modelling 24
 - 3.2.1 Inverse Park and Clarke transforms 25
 - 3.2.2 MATLAB modelling 26
 - 3.3 VSC modelling 31
 - 3.3.1 Current Loop Controller 33
 - 3.3.2 Voltage Controller 35
 - 3.3.3 Phase Locked Loop 35
 - 3.4 Fault Ride Through modelling 38
 - 3.4.1 Stage 1: ride-through control during a fault 39
 - 3.4.2 Stage 2: Post fault recovery control 39
 - 3.4.3 MATLAB Modelling 41

- 4 CHAPTER 4: Model validation and results** **45**
- 5 CHAPTER 5: Conclusions and future work** **55**

 - 5.1 Future work 55

- A Appendix** **57**

 - A.1 Cp calculation 57
 - A.2 Model Variables 60
 - A.3 Simulink designs 62

- Bibliography** **69**

List of Figures

1.1	Installed power in 2020.[1]	9
1.2	Total cumulative power in MW by the end of 2020.[1]	10
1.3	YoY addition to installed capacity.[4]	10
1.4	Historical development of wind power.[4]	11
2.1	Fault Ride-Through capability.[7]	13
2.2	FRT capability for different countries [7]	14
2.3	Reactive power requirements for different countries in EU.[9]	15
2.4	SDBR dynamics of the PMSG wind turbine.[17]	16
2.5	Control scheme of the CBFCL for the PMSG wind turbine [17].	19
2.6	Equivalent CBFCL [19].	19
2.7	Equivalent CBFCL for off-state [19].	20
2.8	Control scheme of the BFCL [19].	20
3.1	Variable-speed wind turbine power curve. [20]	23
3.2	TOP: Direct driven topology, BOTTOM: Hybrid transmission. [22]	23
3.3	Representation of the Inverse Park transform. [22]	26
3.4	C_p curve for the modelled turbine	27
3.5	Power output vs rotor speed at different wind speeds	27
3.6	Model calculation for u_d, u_q	28
3.7	Simulation model for the current stator	28
3.8	Simulation model for the electromagnetic torque	29
3.9	Voltage transformation from abc to dq reference.	29
3.10	Current transformation from dq to abc axis reference.	30
3.11	i_d calculation	30
3.12	i_q calculation	30
3.13	VSC simplification. [21]	31
3.14	Equivalent model from the AC part for the VSC.[21]	32
3.15	Control scheme of a VSC for a wind turbine.[21]	33
3.16	Current Loop Controller diagram. [21]	33
3.17	Voltage Controller diagram. [21]	35
3.18	Voltage Controller diagram. [21]	36
3.19	VSC complete model with grid side and machine side	37
3.20	Generic FRT response waveforms.[17]	38
3.21	Design of active and reactive current reference on the FRT.[17]	39
3.22	Active current controller designed in MATLAB.	41
3.23	Reactive current controller designed in MATLAB.	42
4.1	Grid code requirements in Spain [25].	46
4.2	C_p curve for the modelled turbine	46
4.3	Simulated PMSG turbine under nominal conditions.	47

4.4	i_q simulation for wind speed changes.	48
4.5	i_q detail simulation for wind speed changes.	48
4.6	i_d simulation for wind speed changes.	49
4.7	i_d detailed simulation for wind speed changes.	49
4.8	Fault implementation to the machine side.	50
4.9	Fault detail.	50
4.10	Current flow through fault branch.	51
4.11	MCS current when the fault occurs at $t=2s$	51
4.12	Reactive current at $t=2s$	52
A.1	Full PMSG MODEL	63
A.2	Aerodynamic calculations	64
A.3	Electromagnetic torque calculations	65
A.4	Torque calculations	66
A.5	Full model	67

List of Tables

2.1	Different FRT capabilities for wind turbine in different countries [7].	14
2.2	DFIG and PMSG comparison.[10]	15
3.1	Different control principles and important parameters at each FRT control stage. [17]	38
4.1	WT parameters for 1.5 MW type-4 WT. [23]	45
4.2	PI parameters for the VSC controller. [21]	45

Acronyms/Abbreviations

2D	Two-Dimensional
3D	Three-Dimensional
AC	Alternate Current
AEP	Annual Energy Production
BFCL	Bride Fault Current Limiter
CBFCL	Capacitive Bridge Fault Current Limiter
DC	Direct Current
DEERS	Distributed Energy Resources
DFIG	Doubly-Feed Induction Generator
DQ	Direct-Quadrature
DS	Direct System
ESS	Energy Storage System
FACTS	Flexible AC Transmission Systems
FRT	Fault Ride-Through
GWEC	Global Wind Energy Council
LVRT	Low Voltage Ride Through
MPPT	Maximum Power Point Tracking
PLL	Phase Locked Loop
PMSG	Permanent Magnet Synchronous Generator
RE	Renewable Energy
SDBR	Series Dynamic Braking Resistor
STATCOM	Static Synchronous Compensator
TS	Transmission System
VSC	Voltage Source Converter
WT	Wind Turbine
YoY	Year-over-Year

1 CHAPTER 1: Introduction

Worldwide demands and energy consumption are rapidly increasing because of the exponential growth of the population, technology modernization and industrialization. This rapid growth has required different technologies to be applied in different countries in order to increase the electrification rate. Distributed energy resources (DERs) are being incorporated to the utility grid as a common method due to various reasons: low maintenance requirements, economic, cost saving and environmental impact.

Wind energy has become a powerful energy source in the last years, based on the Global Wind Energy Council (GWEC) 2020 report, the accumulate installed power capacity worldwide reached 742,689 MW in 2020 [1][2].

Even onshore wind power is still the key player in the wind industry (707.396 MW by the end of 2020) offshore wind power is rapidly gaining importance in the future of the renewable energies in Europe [3] and it will be a key player in the next years as the share of renewable energies increases leaving the major production weight to the colossal wind turbines to be installed in the seas. By the end of 2020 a total of 35.196 MW had been installed. Even UK is the leader on the industry, this recent years Netherlands (Figure 1.1) have been increased its installed capacity as new concepts have been developed and tested in its shore. Figure 1.2 shows as Europe is the leader on this kind of installations as it is really investing in a lot of projects and concepts in its seas. Moreover as the urban pressure is increasing it is clearer that the solution lies in offshore the energy sources, especially wind as it requires vast amount of land for its farms.

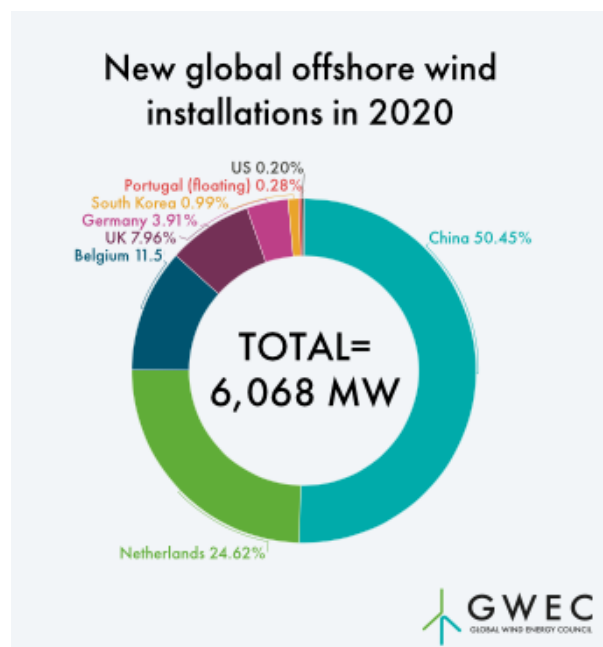


Figure 1.1: Installed power in 2020.[1]

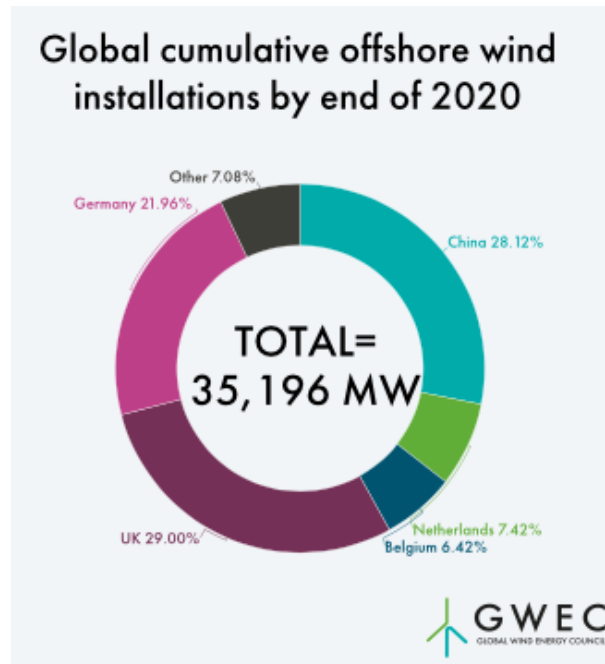


Figure 1.2: Total cumulative power in MW by the end of 2020.[1]

Figure 1.3 clearly shows how the Year-Over-Year (YoY) addition in Asia has been overcoming the European capacity increase, as policies are still slowing down the projects to be developed in some countries with huge availability of Offshore wind energy. Despite of that it is clearly shown that the technology is taking off and it will be a need in the future of the renewable energies.

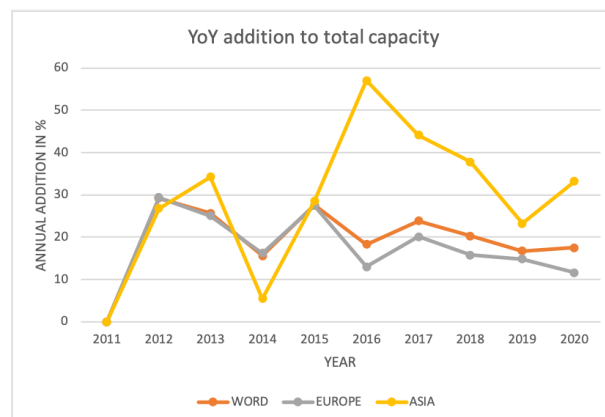


Figure 1.3: YoY addition to installed capacity.[4]

Figure 1.4 supports that the next years will be crucial for this technology and new integration technologies will be needed in order to reduce the impact of VT integration to the utility grid.

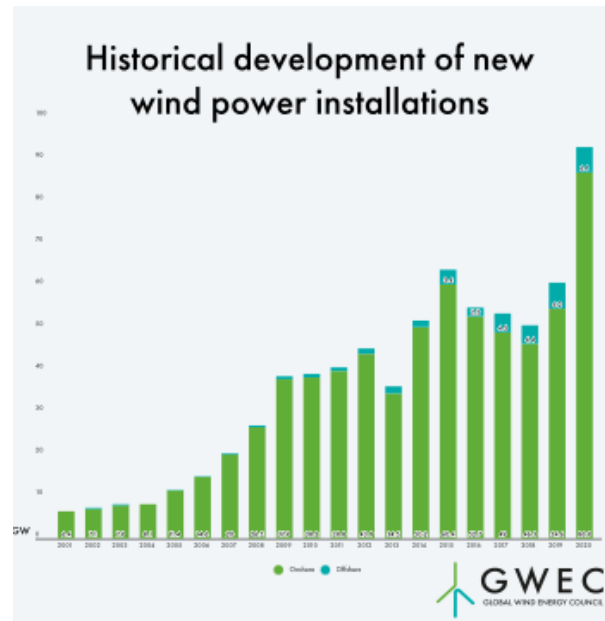


Figure 1.4: Historical development of wind power.[4]

Due to this full-scale voltage source converters (VSC) has appeared as key elements to integrate RE into the grid [5],[6] improving the efficiency of the sources as well ensuring the grid health and capability. Nowadays, VSC is not only used in the renewable energy (RE) generation interconnection but also energy storage systems (ESS) to boost the capacity factor of RE generation.

1.1 Background

Even being an emergent technology with an increasing popularity, wind energy and therefore offshore wind energy are less robust in comparison to other energy production technologies to faults. When a fault in the grid occurs a deep voltage sag occurs. The conventional solution when there was a voltage sag in the grid was to disconnect from the grid in order to avoid damages in the turbine. This was a healthy solution for the turbine but it could cause an unbalance which could lead to a network instability. Nowadays, turbines has to deal with this voltage sags without disconnecting to the grid.

1.1.1 Problem Statement

The increasing of utility-scale of wind power plants has increased the interest in controlling the impact of WT on the electrical power network. The integration of wind power into the grid increases the power system operation complexity affecting the stability of the grid. For that reason it is important to develop further Fault Ride-Through (FRT) strategies and new grid codes have imposed even strict requirements for the wind plants.

1.1.2 Aims and Objectives

The objectives of this thesis is to develop a dynamic model of a permanent magnet synchronous generator (PMSG) type-4 wind turbine (WT) with a back-to-back voltage source converter (VSC) connection, using

Matlab and conduct some different simulations with wind changes and faults on the machine side to validate the model.

1.1.3 Thesis methodology

To develop this thesis various methodologies have been used. As it is based on the design of a model and the previous validation of it, first of all a research phase have been carried out to identify the correct literature review to be used. After this, once done an intense reading of different articles a design phase have been carried out. MATLAB design have been done from the theoretical equations and articles. After this a phase of simulations are done to confirm the good behaviour of the system.

1.1.4 Thesis outline

The thesis has been organized following this structure.

- I Introduction. It presents the global WT situation and the new risks that have appeared as the plants are bigger than before.
- II Chapter 2. It focuses on the literature review of the Fault Ride Through and the different strategies that can be used when a voltage sag occurs.
- III Chapter 3. In this chapter the reader will find the full design of the Type 4 wind turbine. First of all an aerodynamic modelling is presented with the basic equations, then the modelling of the PMSG is presented with the different simulation models developed in Matlab. The next step is to design the full converter of the turbine, in this case the voltage source converter (VSC). Finally the control part of the Fault Ride Through (FRT) is developed.
- IV Chapter 4. In this chapter different simulations are carried out to verify the correct behaviour of the turbine and its correct recovery from the fault.
- V Finally, a summary of conclusions and future work will be presented.

2 CHAPTER 2: Literature Review of Fault Ride-Through

The introduction of fault-ride through capability it is necessary for reliable and stable operations of utility power grids, where there is high level of penetration of wind turbines.

In the grid faults three major issues are identified: fault detection, the control during the fault and the recovery after the fault. As exposed before, in the past the wind turbines were disconnected from the grid when there was a fault, but nowadays they are designed not to only stay connected and recover fast the power generation after a fault clearance, but also provide voltage support and generate capacitance reactive power.[8]

Fault ride-through has been introduced as one of the most important requirements of grid codes regarding the wind farm operations. The capacity of the generation systems of continuing connected to the grid during and after the fault depends a lot on the technology itself and the design of the generation, as the short circuit levels and the characteristics of the control system. In a graphic way, the fault ride-through can be described as shown in Figure 2.1.

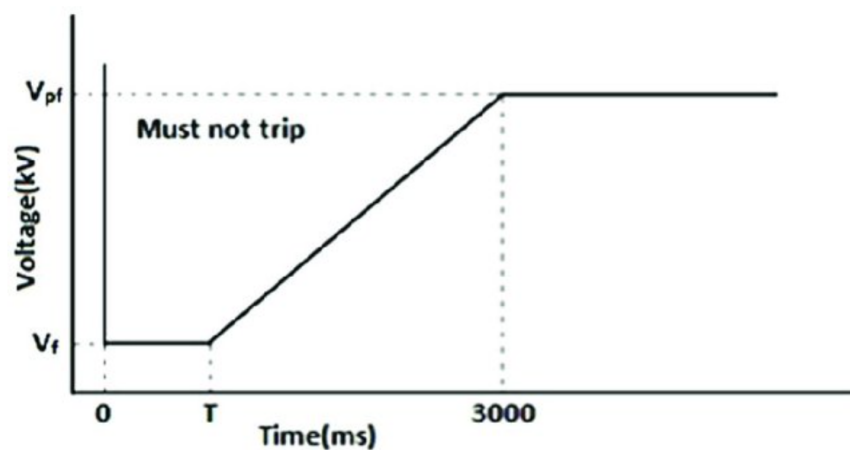


Figure 2.1: Fault Ride-Through capability.[7]

The magnitude of the voltage drop will vary depending on the type and place of the fault, such as single phase ground, three-phase ground, etc. The capability requirements of FRT are different between countries [7]. Table 2.1 summarizes the fault ride-through capabilities in different countries.

The capability clearly defines the voltage drop as well the time to recover from the fault. In some countries the grid codes are very well defined during non-symmetrical faults such as UK, Denmark and Ireland. Figure 2.2 shows the voltage profiles for FRT capability.

Country	Fault ride-through capability			Voltage Level
	<i>Fault duration</i>	<i>Voltage drop level</i>	<i>Recovery time</i>	
Denmark	100 ms	25%	1 s	DS/TS
Ireland	625 ms	15%	3 s	DS/TS
UK	140 ms	15%	1.2 s	DS/TS
Spain	500 ms	20%	1 s	TS
Germany	150 ms	0%	1.5 s	DS/TS
Italy	500 ms	20%	0.3 s	35 Kv
Canada	150 ms	0%	0.18 s	TS
USA	625 ms	15%	2.3 s	TS

Table 2.1: Different FRT capabilities for wind turbine in different countries [7].

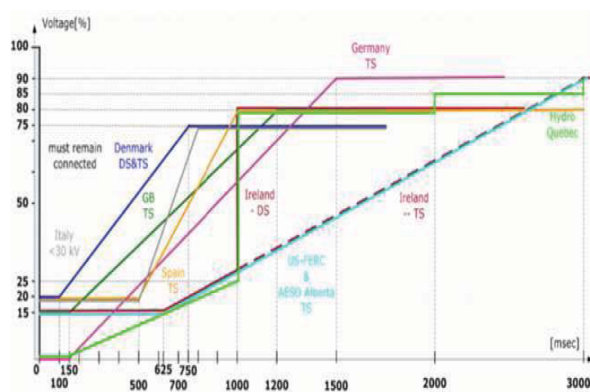


Figure 2.2: FRT capability for different countries [7]

It can be observed that countries as Denmark, Ireland, Germany and UK have different requirements of FRT capability depending on the system: transmission system (TS) and distribution system (DS), while the others only focus on the transmission system only.

The voltage levels range must be very tiny in order to maintain the utility and customers utility, which are configured to work at specific voltage levels. When the fault occurs, the voltage will suffer a drop and fluctuate for a few moments where the WT should be able to inject reactive power to regulate and support the voltage. The effect of injecting reactive power to the grid depends on the short circuit capacity, grid impedance and the total amount of load close to the connection point. Depending on the country the requirements of reactive power to inject in order to compensate the voltage drop will vary, and it usually follows the P-Q diagram shown in Figure 2.3.

Type	Advantages	Disadvantages
DFIG	<p>speed range $\pm 30\%$</p> <p>Small capacity converters</p> <p>Full range control for active and reactive power</p>	Requires gearbox (high maintenance cost)
PMSG	<p>Full speed range</p> <p>No gearbox needed</p> <p>Full range control for active and reactive power</p> <p>Brushless</p>	<p>Full scale converter (more expensive)</p> <p>Multi-pole generator (heavy component)</p> <p>Requires permanent magnets</p>

Table 2.2: DFIG and PMSG comparison.[10]

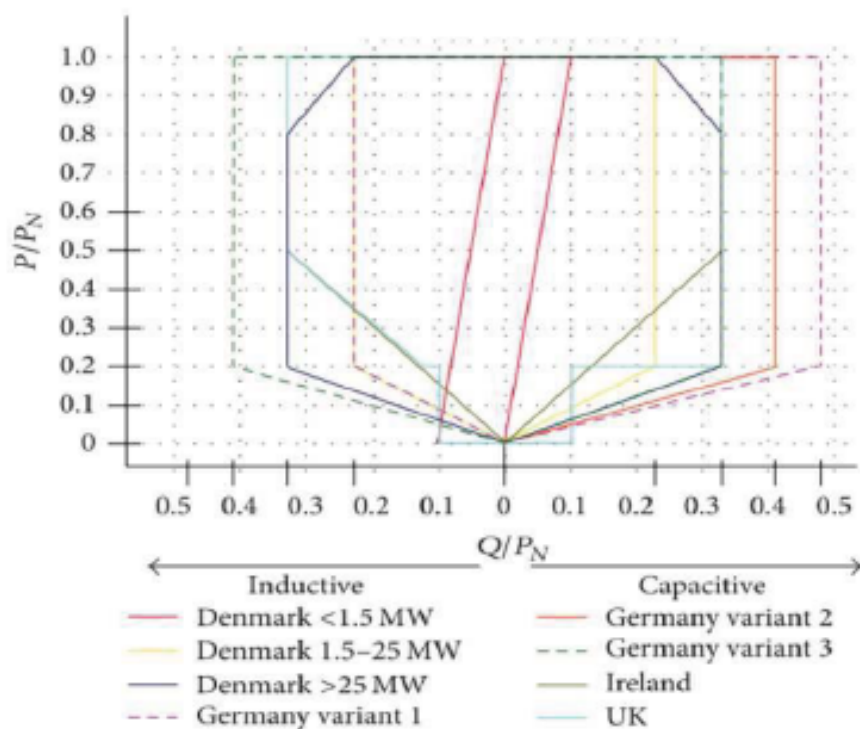


Figure 2.3: Reactive power requirements for different countries in EU.[9]

The security of the power system is a concern for the fault ride through capability, for that reason the improvement of FRT can be achieved by using different strategies.

Depending on the type of turbine FRT solution it differs. Old wind turbines are expensive to re-design, for that reason the better solution is to replace the controlling voltage devices by Flexible AC Transmission Systems (FACTS). The most used turbines nowadays are the PMSG and the doubly-feed induction generator (DFIG) wind turbines. Table 2.2 shows a basic comparison between both models.

As this project is focused on the permanent magnet synchronous generator (PMSG) the FRT strategies exposed will basically focus on this type of turbine.

In the literature, several FRT or Low Voltage Ride Through (LVRT) control strategies for PMSG wind turbines, from peak current limitation (Nasiri and Mohammadi, 2017)[11], active crowbar switch (Yehia et al.,2018)[12], DC-chopper devices (Nasiri et al.,2015)[13], Superconducting Fault Current Limiter (SFCL) (Conroy,2017)[14], Maximum Power Point Tracking (MPPT) (Gencer, 2018)[15]. These strategies for PMSG are simple and cost-effective compared to the use of FACTS devices for old wind turbines like Static Synchronous Compensator (STATCOM)[16].

Among all FRT strategies three of them are the most used in wind turbines. The Series Dynamic Braking Resistor (SDBR), the Capacitive Bridge Fault Current Limiter (CBFCL) and the traditional Bridge Fault Current Limiter (BFCL).

2.1 Series Dynamic Braking Resistor (SDBR) strategy

The basic connection scheme for the SDBR for a PMSG-based wind turbine is shown in Figure 2.4.

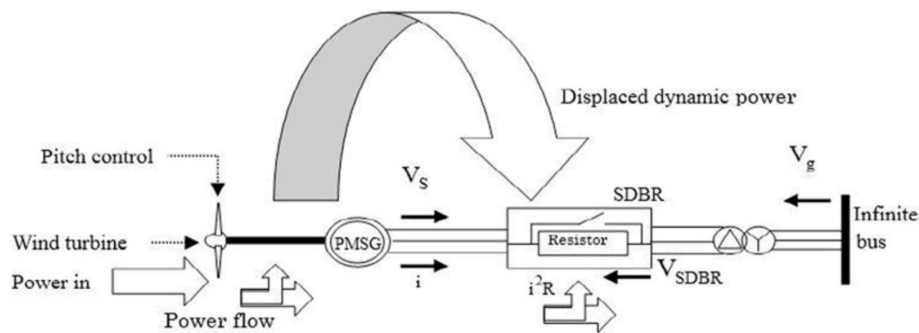


Figure 2.4: SDBR dynamics of the PMSG wind turbine.[17]

This strategy is based on the current control and not the voltage [18]. During nominal operation, when the switch conducts the resistor is bypassed, based on the threshold value of the voltage of the grid. When the fault occurs, the switch is off. During the switching strategy the SDBR will limit the high rotor current while operating, and the excessive active power will be achieved. These effects helps to effectively achieve the balance in the machine side converter (MSC) and the grid side converter (GSC) and therefore reducing the stator current and the DC-link capacitor charging.

The grid side is connected to R and L parameters of the grid. Using Park's transformation, the VSC of the PMSG could be modeled as

$$e_d = -\omega L i_q + L \frac{di_d}{dt} + (R + R_{SDBR}) i_d + 0.5 U_{dc} \beta_d \quad (1)$$

$$e_q = -\omega L i_d + L \frac{di_q}{dt} + (R + R_{SDBR}) i_q + 0.5 U_{dc} \beta_q \quad (2)$$

$$C \frac{dU_{dc}}{dt} = 0.75(i_d \beta_d + i_q \beta_q) - \frac{U_{dc}}{R_L} \quad (3)$$

$$r = \sqrt{\beta_d^2 + \beta_q^2} \quad (4)$$

where i_d and i_q are the derivative current input of the rectifier's axes, β the angular frequency voltage e_d and e_q are the dq voltages of the grid, and the r is the modulation of the signal vector norm, U_{dc} the DC-link voltage, and the R_{SDBR} the effective SDBR resistance. The Park's principle for the transformation for phase-A voltage grid with the dq reference is

$$e_d = E_m \quad (5)$$

$$e_q = 0 \quad (6)$$

where E_m corresponds to the voltage amplitude, e_d and e_q , the d and q source voltages. The rectifier's powers are

$$P_s = \frac{3}{2} E_m i_d \quad (7)$$

$$Q_s = -\frac{3}{2} E_m i_q \quad (8)$$

Considering $e_q = 0$ and $i_q = 0$, the VSC for unity power factor is

$$E_m = L \frac{di_d}{dt} + (R + R_{SDBR})i_d + 0.5U_{dc}\beta_d \quad (9)$$

$$\beta_q = -\frac{2\omega L}{U_{dc}} i_q \quad (10)$$

$$C \frac{dU_{dc}}{dt} = 0.75(i_d \beta_d - \frac{U_{dc}}{R_L}) \quad (11)$$

For a unity power factor of the VSC, β_q vary with the i_q current. Thereby, the capacitor charge is modified by β_d , via d based on (11) and (10). When connecting the SDBR, the equations will be

$$E_m = (R + R_{SDBR})i_d + 0.5U_{dc}\beta_d \quad (12)$$

$$\beta_q = -\frac{2\omega L}{U_{dc}} i_q \quad (13)$$

$$i_d = \frac{4U_{dc}}{3\beta_d R_L} \quad (14)$$

For a load R_L and for a voltage U_{dc} ,

$$6E_m R_L \beta_d - 8(R + R_{SDBR})U_{dc} - 3R_L \beta_d^2 U_{dc} = 0, \text{ for } \beta_d \neq 0 \quad (15)$$

so this two solutions are achieved:

$$\beta_{d1} = \frac{E_m}{U_{dc}} - \sqrt{\left(\frac{E_m}{U_{dc}}\right)^2 - \frac{8(R + R_{SDBR})}{3R_L}} \quad (16)$$

$$\beta_{d2} = \frac{E_m}{U_{dc}} - \sqrt{\left(\frac{E_m}{U_{dc}}\right)^2 - \frac{8(R + R_{SDBR})}{3R_L}} \quad (17)$$

Solution of Equation (16) has very low values for that reason (17) is acceptable by making $\beta_d = \beta_{d2}$, and it would exist if

$$\left(\frac{E_m}{U_{dc}}\right)^2 - \frac{8(R + R_{SDBR})}{3R_L} \geq 0 \quad (18)$$

But

$$P_{dc} \leq P_{dcmax} \quad (19)$$

where P_{dcmax} is the maximum of PSMG which can be expressed as

$$P_{dc} = \frac{3}{2}E_m i_d - \frac{3}{2}(R + R_{SDBR})i_d^2 \quad (20)$$

If $dP_{dc}/d i_d = 0$, the maximum intensity transferred to the dc would be

$$i_d = i_{dcmax} = \frac{E_m}{2(R + R_{SDBR})} \quad (21)$$

By substituting the last two equations we get

$$P_{dcmax} = \frac{3E_m^2}{8(R + R_{SDBR})} \quad (22)$$

and the VSC operation is possible when

$$P_{dc} \leq P_{dcmax} \rightarrow \left(\frac{E_m}{U_{dc}}\right)^2 - \frac{8(R + R_{SDBR})}{3R_L} \geq 0 \quad (23)$$

So the grid input maximal power P_{dcmax} can be obtained from 8 and 22

$$P_{smax} = \frac{3E_m^2}{4(R + R_{SDBR})} \quad (24)$$

2.2 Capacitive Bridge Fault Current Limiter (CBFCL) strategy

CBFCL circuit is formed by four diodes with a switching circuit of a DC reactor [19]. As we can see in Figure 2.5 the capacitor C_{sh} with a series resistor R_{sh} made up the shunt path. Moreover, two fast recovery diodes (D_5 and D_6). The switching strategy is similar to the SDBR strategy.

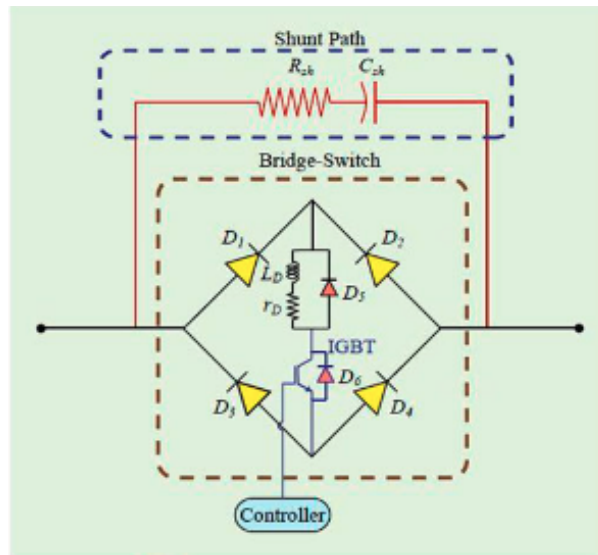


Figure 2.5: Control scheme of the CBFCL for the PMSG wind turbine [17].

In order to simplify the operation of the capacitor in a high voltage range, the control of the PWM is a function of V_C , V_S , V_L at the equivalent circuit shown in Figure 2.6.

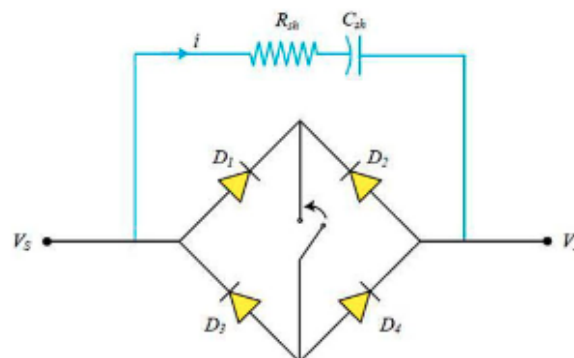


Figure 2.6: Equivalent CBFCL [19].

The equations for the equivalent model are based on the Kirchoff's law,

$$C_{sh} \frac{dV_C}{dt} = i \quad (25)$$

$$i = \frac{V_s - V_C - V_L}{R_{sh}} \quad (26)$$

$$C_{sh} \frac{dV_C}{dt} = \frac{V_s - V_C - V_L}{R_{sh}} \quad (27)$$

Arranging equation (27)

$$\frac{dV_C}{dt} = -\frac{V_C}{R_{sh}C_{sh}} + \frac{V_s}{R_{sh}C_{sh}} + \frac{V_L}{R_{sh}C_{sh}} \quad (28)$$

where the different parameters correspond to the capacitor, and the current in the shunt path. On the other hand, the off-state equation based on the Kirchoff's law as shown in Figure 2.8

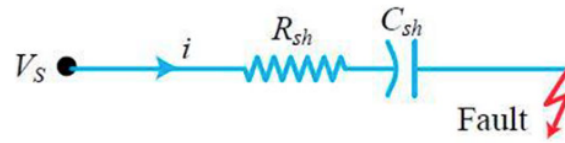


Figure 2.7: Equivalent CBFCL for off-state [19].

So,

$$C_{sh} \frac{dV_C}{dt} = i \quad (29)$$

Following the Ohm's law it is possible to express the current during a fault as

$$i = \frac{V_s - V_C}{R_{sh}} \quad (30)$$

$$C_{sh} \frac{dV_C}{dt} = \frac{V_s - V_C}{R_{sh}} \quad (31)$$

which leads to

$$\frac{dV_C}{dt} = -\frac{V_C}{R_{sh}C_{sh}} + \frac{V_s}{R_{sh}C_{sh}} \quad (32)$$

2.3 Bridge Fault Current Limiter (BFCL) strategy

Similar strategy to the last one presented, in BFCL the scheme follows as seen in Figure

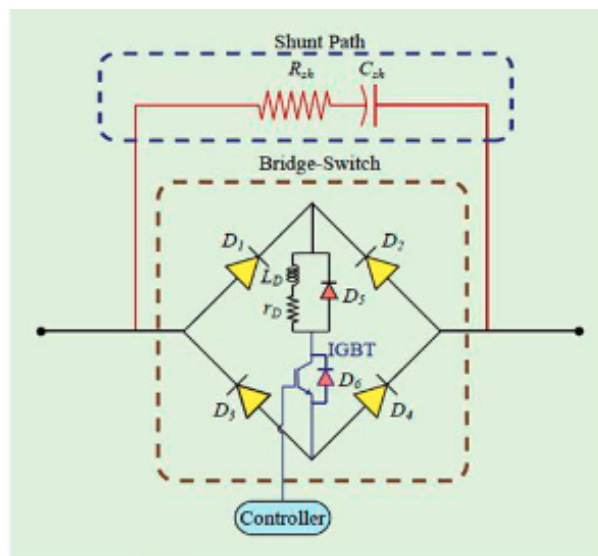


Figure 2.8: Control scheme of the BFCL [19].

The main part is formed by a typical bridge circuit of four diodes and a shunt part made of the inductor and resistor in series. Moreover, an IGBT switch is connected in series with an inductor. In this device, the L_{dc} inductor is a DC reactor as the current only flows in one direction during the positive and negative half cycle on the alternating current. The basic working principle of the BFCL is that during the steady state the current flows through D_1 - L_{dc} - R_{dc} -IGBT- D_4 path for the positive half cycle and D_3 -IGBT- R_{dc} - L_{dc} - D_2 path for the negative half cycle.

The basic control strategy works based on the threshold grid voltage.

3 CHAPTER 3: Modelling and control - Type 4 turbine

In this chapter the modelling of the dynamics of the mechanical system of the turbine will be analyzed. It will include an aerodynamic modelling of the generator, a linearized version of the power system and finally the control of the wind turbine.

In this thesis a variable wind speed turbine is being analyzed. This kind of turbines has the advantage to follow the variation of the wind speed during the day and to produce more energy under normal operation at low wind speed, through the MPPT. The basic principle follows that when the wind speed is more high than the rated wind speed, the turbine will work under constant power. In Figure 3.1 Region II shows that the turbine output follows an MPPT curve until it achieves the rated power.

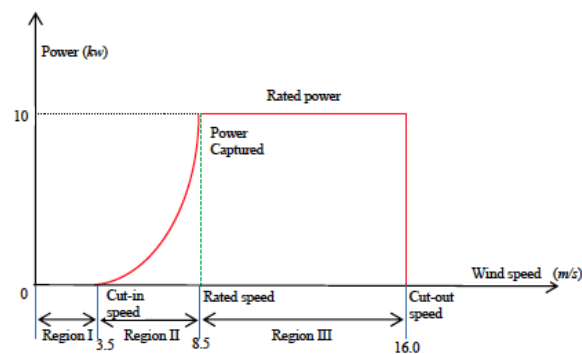


Figure 3.1: Variable-speed wind turbine power curve. [20]

As explained before, the variable-speed wind turbine of this thesis uses a synchronous generator, more precisely a PMSG.

In general there are two different typologies for turbines with PMSG: hybrid transmission (using one stage planetary gear) or direct driven (without gearbox) as illustrated in Figure 3.2.

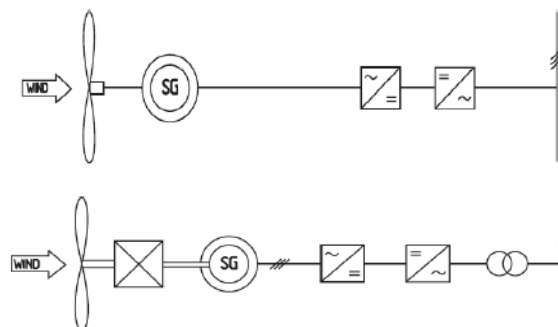


Figure 3.2: TOP: Direct driven topology, BOTTOM: Hybrid transmission. [22]

Even some differences in the frequency and amplitude of the voltage output, they both require a full power conversion for grid connection, as illustrated in Figure 3.2.

3.1 Wind turbine modelling

This section will include all the modelling steps of the wind turbine itself.

3.1.1 Aerodynamics modelling

The power from a wind turbine at the rotor can be expressed as:

$$P_t = \frac{1}{2} C_p(\lambda) \rho R^2 v^3 \quad (33)$$

where $C_p(\lambda)$ it corresponds to the power coefficient, which is a representation of the aerodynamic performance of the wind turbine rotor. C_p is function of the blade tip speed ratio λ as stated by Borowy Bogdan S. and Salameh Ziyad M. 1997:

$$\lambda = \frac{R\omega}{v} \quad (34)$$

There is not a fix $C_p(t)$ curve as is specific for each turbine and it depends particularly in the blade design.

The aerodynamic torque can be expressed as

$$T_t = \frac{P_t}{\omega} = \frac{1}{2} \frac{C_p(\lambda)}{\lambda} \rho \pi R^2 v^2 \quad (35)$$

And the power output at the generator can be expressed as

$$P_G = \frac{1}{2} \nu C_p(\lambda) \rho \pi R^2 v^3 \quad (36)$$

where ν represents the total efficiency of the mechanical transmission system and the generator.

3.2 PMSG modelling

PMSG modelling is not an easy task and it requires, to make some assumptions in order to simplify the model:

- Permanent magnet conductivity is zero
- No field current dynamics
- The saturation is neglected
- EMF is sinusoidal
- Hysteresis losses are negligible

Given the assumptions needed, the PMSG can be modelled as follows in the direct-quadrature (DQ) coordinate system

$$V_{qs} = -r_s i_{qs} + L_{qs} \frac{d}{dt} i_{qs} - \omega_r L_{ds} i_{ds} + \omega_r \frac{dy}{dx} \psi_{ds} \quad (37)$$

$$V_{ds} = -r_s i_{ds} + L_{ds} \frac{d}{dt} i_{ds} + \omega_r L_{qs} i_{qs} \quad (38)$$

where

- V_{xs} corresponds to the stator voltage in the dq-axis
- i_{xs} corresponds to the stator current in the dq-axis
- ω_r corresponds to the angular velocity of the generator
- r_s corresponds to the equivalent resistance of the stator winding
- L_{xs} corresponds to the stator equivalent inductance in the dq-axis
- $d/dt \psi_{ds}$

Then, the electromagnetic torque can be expressed as

$$T_e = \frac{3P}{4} [i_{ds}i_{qs}(L_{ds} - L_{qs}) + i_{qs} \frac{d}{dt} \psi_{ds}] \quad (39)$$

where T_e represents the electromagnetic torque in Nm and P the pole number at the generator stator. It is possible to obtain the relationship between the angular velocity of the rotor and the mechanical angular velocity of the wind turbine as follows

$$\omega = \frac{2\omega_r}{PG} \quad (40)$$

$$\frac{d}{dt} \omega_r = \frac{P}{2J} (T_m - T_e) \quad (41)$$

where

- T_m is the input mechanical torque (Nm)
- G is the gear ratio
- J is the inertia of the generator (kgm^2)

The input torque to the generator it can be easily obtained as

$$T_m = \frac{T_t}{G} \quad (42)$$

In case of a PMSG direct-driven wind turbine, as the one studied in this project, $G=1$, and $T_m = T_t$.

3.2.1 Inverse Park and Clarke transforms

Both transformations are required to implement a 3-phase AC output from the generator model. The transformation from the axis reference frame ($\alpha\beta$) to the rotating reference frame (dq) is called Park transform. The inverse transformation from the 3-phase reference frame to the 2-phase stator axis ($\alpha\beta$) is called the Clarke transform.

Figure 3.3 illustrates the inverse Park transform.

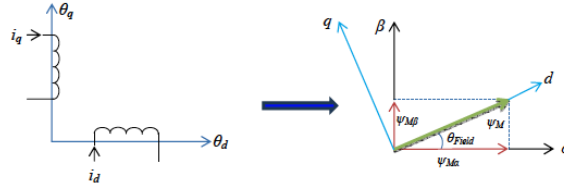


Figure 3.3: Representation of the Inverse Park transform. [22]

Figure 3.3 assumes that $\alpha\beta$ frame has an angle ϑ_{Field} with the dq frame that can be expressed as

$$\begin{bmatrix} \alpha \\ \beta \end{bmatrix} = \begin{bmatrix} \cos(\theta_{\text{Field}}) & -\sin(\theta_{\text{Field}}) \\ \sin(\theta_{\text{Field}}) & \sin(\theta_{\text{Field}}) \end{bmatrix} \begin{bmatrix} d \\ q \end{bmatrix} \quad (43)$$

Finally it is possible to obtain the inverse Clarke transform as

$$\begin{bmatrix} V_a \\ V_b \\ V_c \end{bmatrix} = \begin{bmatrix} 1 & 0 \\ -\frac{1}{2} & \frac{\sqrt{3}}{2} \\ -\frac{1}{2} & -\frac{\sqrt{3}}{2} \end{bmatrix} \begin{bmatrix} \alpha \\ \beta \end{bmatrix} \quad (44)$$

3.2.2 MATLAB modelling

As exposed before, the power coefficient of the wind turbine depends on each model. There are many different ways to simulate the curve of the $C_p(\lambda)$. In order to get the graph an iterative process is needed which can be really complex. In this project, the following polynomial approximation has been used

$$C_p(\lambda) = a_1 + a_2\lambda + a_3\lambda^2 + a_4\lambda^3 + a_5\lambda^4 + a_6\lambda^5 \quad (45)$$

Figure 4.2, shows the shape of the calculated $C_p(\lambda)$ based on the equation (45).

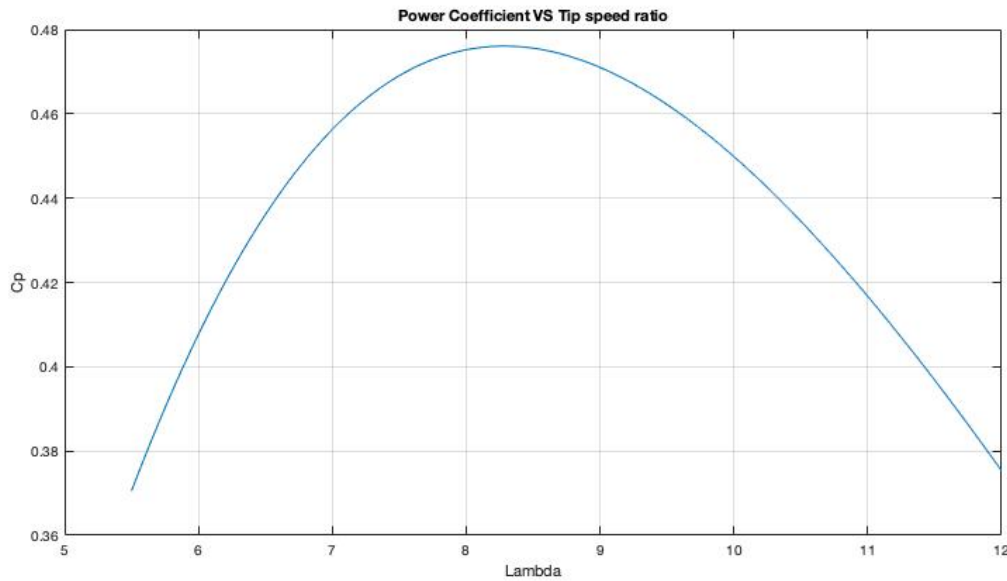


Figure 3.4: C_p curve for the modelled turbine

It also shows how the maximum C_p at rated wind power is 0.476.

Moreover it is possible to extract the relation between the output power and the rotor speed at different wind speed combining (45) and (36).

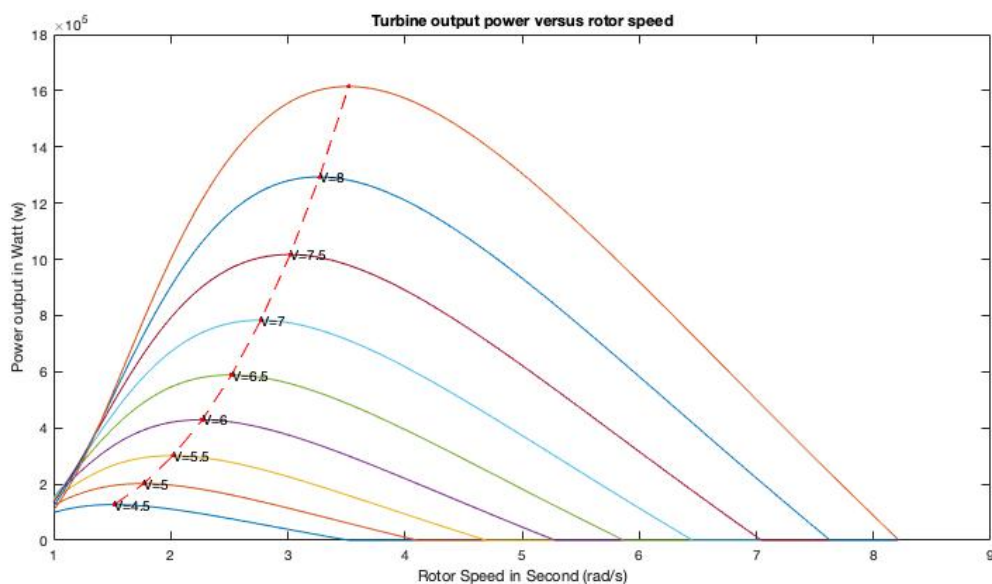


Figure 3.5: Power output vs rotor speed at different wind speeds

Red line shows the MPPT for each wind speed.

Once the aerodynamic part is already detailed the PMSG, can be designed using equations presented

before in Section 3.2.

Figure shows the model that implements the different transforms from the 3-phase balance frame to the DQ-coordinate system through the Park transform.

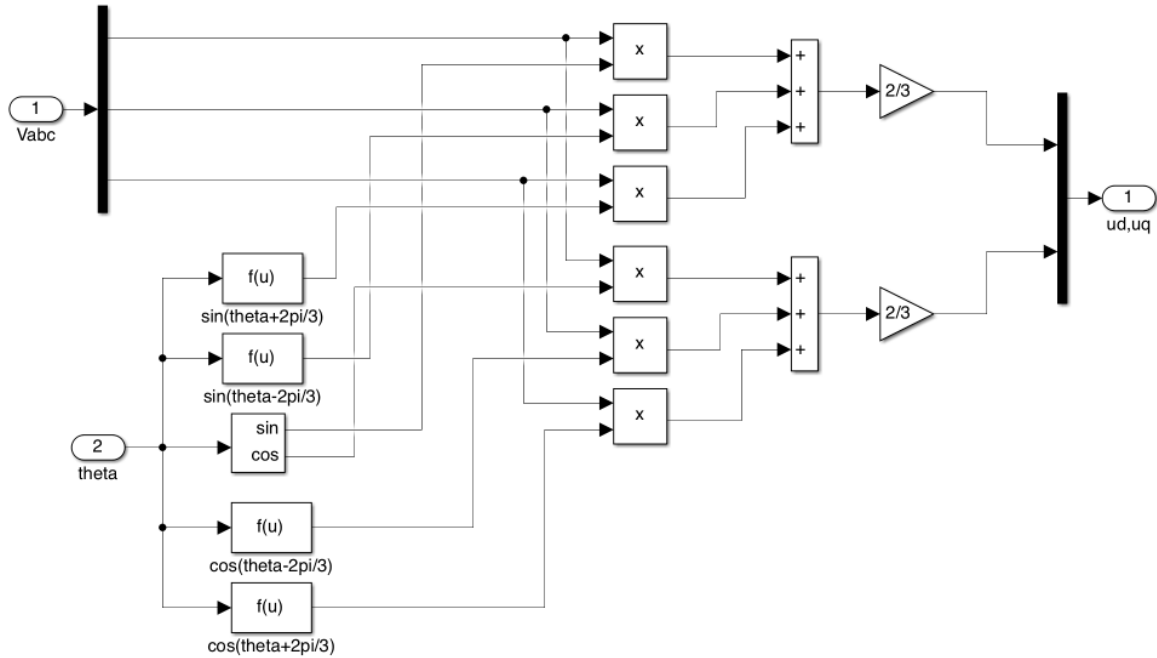


Figure 3.6: Model calculation for u_d, u_q

Once the stator voltage in the dq-axis is calculated through Park transform, it is possible to obtain the stator current in the DQ-coordinate system from the equations (37) and (38).

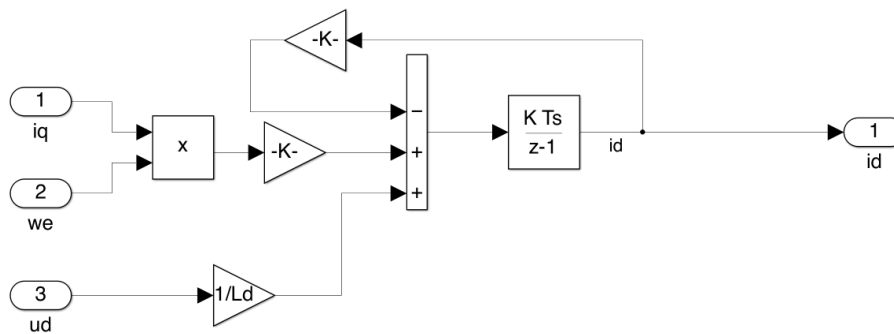


Figure 3.7: Simulation model for the current stator

Finally from 39 the electromagnetic torque can be obtained, as it shows the model.

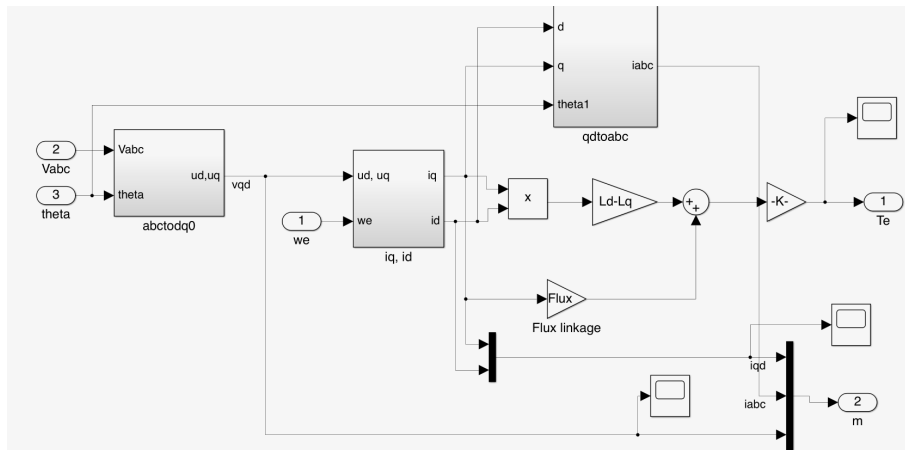


Figure 3.8: Simulation model for the electromagnetic torque

Previous figure shows a generic scheme of the model for the PMSG wind turbine.

Figure 3.9 shows the transformation of the voltage V_{abc} to u_{dq} reference in order to compute both $i_{d,q}$.

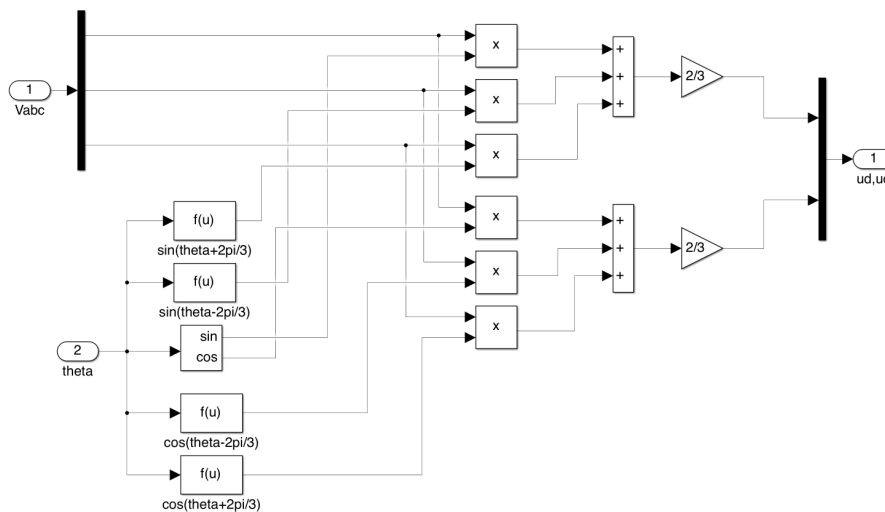


Figure 3.9: Voltage transformation from abc to dq reference.

Figure 3.10 it is possible to see the model created to compute the current in the axis reference frame.

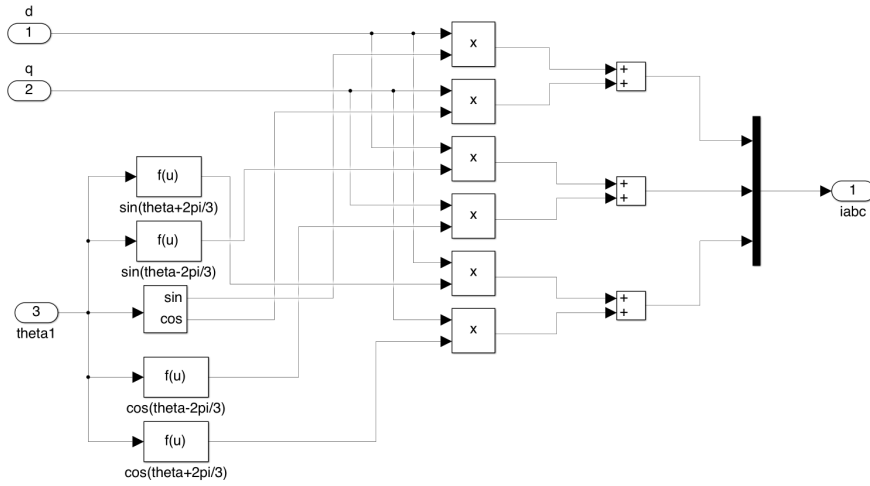


Figure 3.10: Current transformation from dq to abc axis reference.

Once the required previous transformations are done it is possible to compute the current in the rotating reference frame (dq) as shows Figure 3.11 and Figure 3.12.

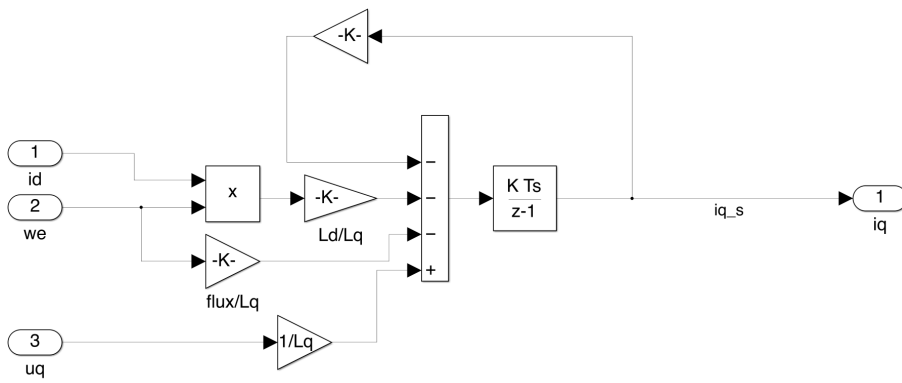


Figure 3.11: i_d calculation

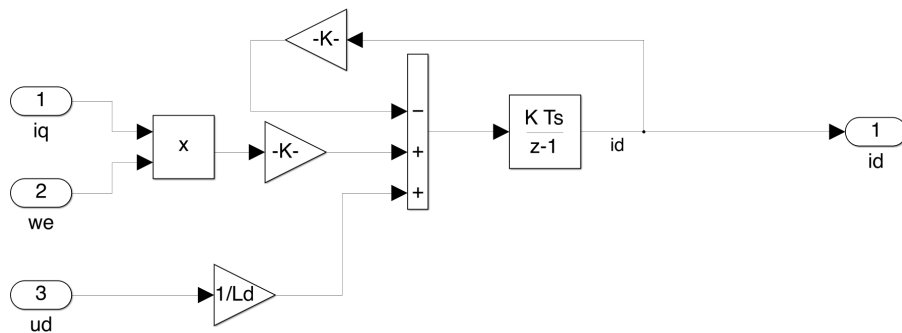


Figure 3.12: i_q calculation

3.3 VSC modelling

From the different converter options available in the market the VSC has been chosen because it allows to have an independent control over the active power and the reactive power. The correct modulation of the IGBT allows to generate the desired 3-phase voltage.

In order to simplify the study and control of the VSC the six IGBTs from the original model are replaced by three constant voltage sources as shown in Figure 3.13.

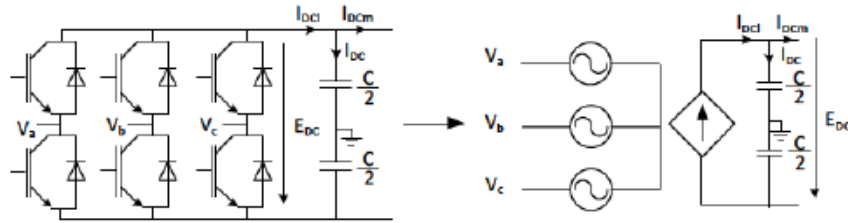


Figure 3.13: VSC simplification. [21]

The simplified model splits the converter into two parts: the AC part and the DC part. In the AC part, the converter is modelled as a voltage source, while the DC part is modelled as a current source, as seen in Figure 3.13. The current source from the DC part reflects the active power exchanged between the AC and the DC part and assures the power balance of the system.

The current from the DC part neglecting the power conversion losses as,

$$I_{DCl} = \frac{P_{AC}}{E_{DC}} \quad (46)$$

where,

- E_{DC} , is the voltage of the DC part
- P_{AC} , corresponds to the active power exchanged between the VSC and the AC grid.

Through the voltage equations it is possible to obtain an equivalent scheme of the AC part of the converter in order to simplify the study,

$$\begin{bmatrix} v_{zq} \\ v_{zb} \\ v_{zc} \end{bmatrix} - \begin{bmatrix} v_{la} \\ v_{lb} \\ v_{lc} \end{bmatrix} - (v_{ol} - v_{oz}) \begin{bmatrix} 1 \\ 1 \\ 1 \end{bmatrix} = \begin{bmatrix} r_l & 0 & 0 \\ 0 & r_l & 0 \\ 0 & 0 & r_l \end{bmatrix} \begin{bmatrix} i_a \\ i_b \\ i_c \end{bmatrix} + \begin{bmatrix} l_l & 0 & 0 \\ 0 & l_l & 0 \\ 0 & 0 & l_l \end{bmatrix} \frac{d}{dt} \begin{bmatrix} i_a \\ i_b \\ i_c \end{bmatrix} \quad (47)$$

where,

- V_{za}, V_{zb}, V_{zc} , corresponds to the instant grid voltage on the abc reference

- v_{1a}, v_{1b}, v_{1c} , corresponds to the instant converter voltage on the abc reference
- i_a, i_b, i_c , corresponds to the instant current on the abc reference
- $v_{10}-v_{z0}$, corresponds to the difference between the converter and the neutral phase of the grid

From this equations the diagram shown on Figure 3.14 can be extracted.

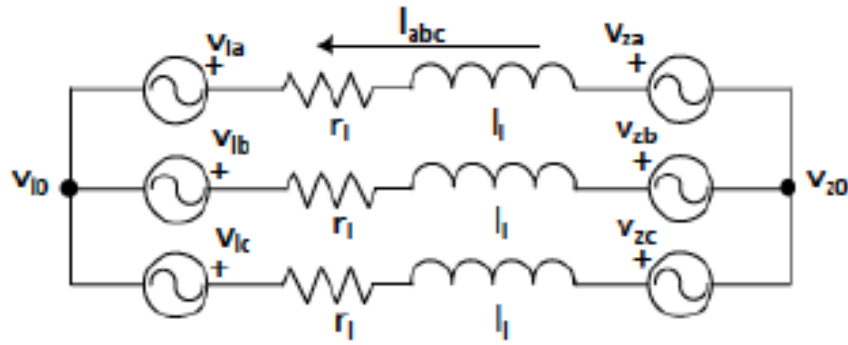


Figure 3.14: Equivalent model from the AC part for the VSC.[21]

In cases where there is no neutral phase, it can be extracted that $v_{10}-v_{z0}=0$ and the voltage equations can be simplified to

$$\begin{bmatrix} v_{zq} \\ v_{zd} \end{bmatrix} - \begin{bmatrix} v_{1q} \\ v_{1d} \end{bmatrix} = \begin{bmatrix} r_l & l_l \omega_e \\ -l_l \omega_e & r_l \end{bmatrix} \begin{bmatrix} i_q \\ i_d \end{bmatrix} + \begin{bmatrix} l_l & 0 \\ 0 & l_l \end{bmatrix} \frac{d}{dt} \begin{bmatrix} i_q \\ i_d \end{bmatrix} \quad (48)$$

As it says in [21], wind turbine can be simplified as current source. The converter control diagram can be found on Figure 3.15, based on a two level control scheme. The internal controller allows to regulate the AC current in the $qd0$ reference, while the external controller allows to regulate the DC voltage in the same reference.

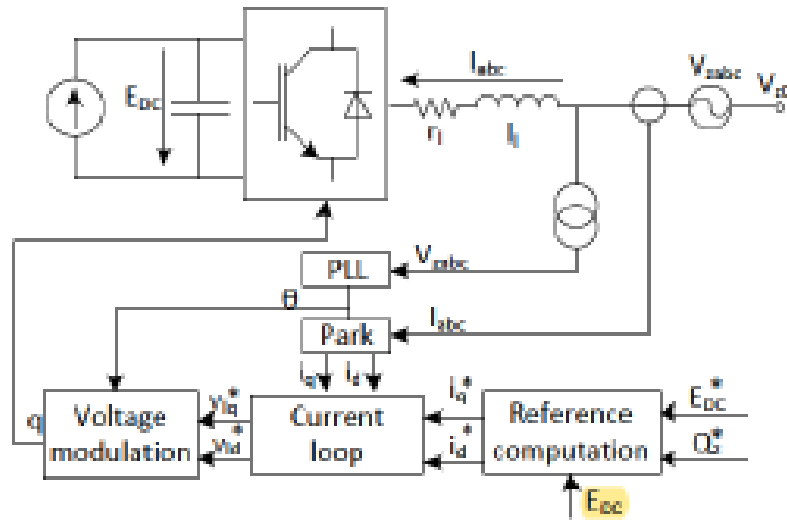


Figure 3.15: Control scheme of a VSC for a wind turbine.[21]

As both controllers works on the qd0-reference, through the reference rotation to adjust the electrical angle of the grid. For that reason the Phase Locked Loop (PLL) is required, at it allows the tracking of the grid angle. This angle allows to compute the inverse Park transform, well needed for the system.

3.3.1 Current Loop Controller

Current Loop Controller allows to compute the voltage that the VSC needs to apply ($v_{l,q}$ i $v_{l,d}$) to ensure that the current that flows through the converter is the same the reference current of the controller (i_q^* i_d^*).

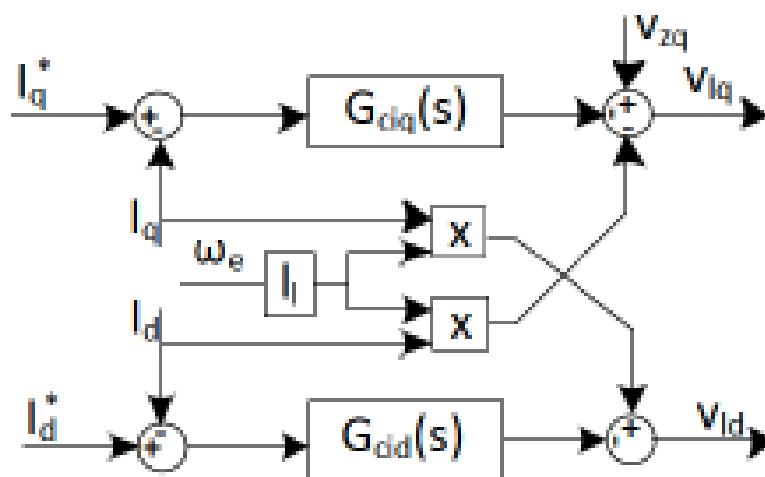


Figure 3.16: Current Loop Controller diagram. [21]

If $v_{zd}=0$ is assumed, the voltage equations can be written as

$$\begin{bmatrix} v_{zq} \\ 0 \end{bmatrix} - \begin{bmatrix} v_{lq} \\ v_{ld} \end{bmatrix} = \begin{bmatrix} r_l & l_l \omega_e \\ -l_l \omega_e & r_l \end{bmatrix} \begin{bmatrix} i_q \\ i_d \end{bmatrix} + \begin{bmatrix} l_l & 0 \\ 0 & l_l \end{bmatrix} \frac{d}{dt} \begin{bmatrix} i_q \\ i_d \end{bmatrix} \quad (49)$$

where it is possible to see the relation between components q and d of the current and voltage, which can be controlled independently.

Decoupling the components q and d of the voltage and integrating them inside the previous equations, the following voltage equations are obtained

$$\begin{bmatrix} v_{lq} \\ v_{ld} \end{bmatrix} = \begin{bmatrix} -\hat{v}_{lq} + v_{zq} - l_l \omega_e i_{ld} \\ -\hat{v}_{ld} + l_l \omega_e i_{lq} \end{bmatrix} \quad (50)$$

Then, if the Laplace transform is applied, the transfer functions between controller and converter can be written as

$$\frac{\hat{v}_{lq}(s)}{i_q(s)} = \frac{1}{l_l s + r_l} \quad (51)$$

$$\frac{\hat{v}_{ld}(s)}{i_d(s)} = \frac{1}{l_l s + r_l} \quad (52)$$

The controller for the previous transfer functions can be designed using the Internal Model Control technique, which allows to obtain the following controller

$$G_{ciq}(s) = G_{cid}(s) = \frac{K_p s + k_i}{s} \quad (53)$$

With the respective constants,

$$K_p = \frac{l_l}{\tau} \quad (54)$$

$$K_i = \frac{r_l}{\tau} \quad (55)$$

which will be defined in the simulations.

Finally, to obtain the i_q^* and i_d^* reference values from active and reactive power (P^* , Q^*), the following power theory is applied,

$$P^* = \frac{3}{2}(v_{zq} i_q^* + v_{zs} i_d^*); Q^* = \frac{3}{2}(v_{zq} i_d^* - v_{zd} i_q^*) \quad (56)$$

As defined before, $v_{zd}=0$ so i_q^* and i_d^* can be obtained as

$$i_q^* = \frac{2 P^*}{3 v_{zq}} \quad (57)$$

$$i_d^* = \frac{2 Q^*}{3 v_{zq}} \quad (58)$$

Q^* will be fixed and the active power P^* will adjust in order to regulate the continuous voltage.

3.3.2 Voltage Controller

The function of this controller is to control the balance between the generated power of the wind turbine and the power injected to the grid. This part allows to obtain the values for P^* and i_q^* as shown in Figure 3.17.

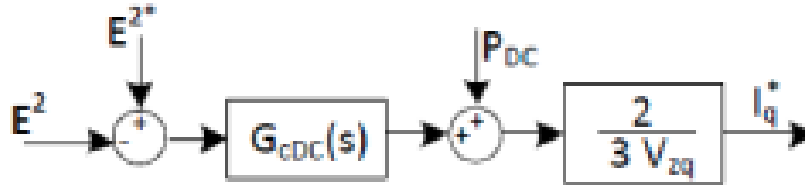


Figure 3.17: Voltage Controller diagram. [21]

E^{2*} corresponds to the E_{DC}^{2*} which is compared to the real value of E_{DC}^2 obtained at the condenser terminals in the continuous part. Finally at the output of the controller, it is obtained the active power injected P_{DC}^* .

This energy is added to the measured before the condenser (P_{DC}) which allows to obtain active power P^* to compute i_q^* .

$$P^* = P_C^* + P_{DC} \quad (59)$$

The PI values can be obtained as,

$$K_{P,DC} = C\xi_E\omega_E \quad (60)$$

$$K_{i,DC} = \frac{C\omega_E^2}{2} \quad (61)$$

where C is the condenser from the dc part of the converter, ω_E the desired angular velocity in the voltage loop and ξ_E corresponds to the *damping ratio* of the loop.

3.3.3 Phase Locked Loop

Phase Locked Loop (PLL) its a system where the phase and frequency are feedback-able. It is used to determine the angle and angular velocity of the grid. The other objective of this controller is to stabilize v_d to 0, reason why it has been assumed that $v_{zd}=0$. The general diagram for a PLL is shown in Figure 3.18 .

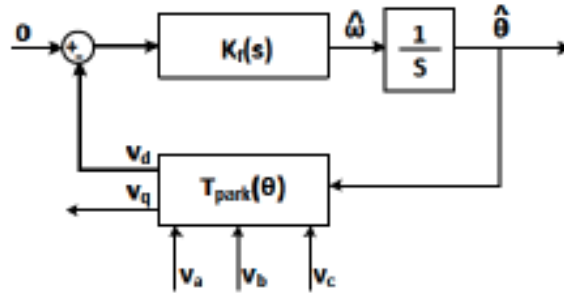


Figure 3.18: Voltage Controller diagram. [21]

It consists on the feedback of the d component of the voltage that is filtered by a PI controller. The output of this controller is the estimated angular velocity of the grid and its angle (through the integrer).

Through linearization it is possible to obtain the system equations, required to obtain the constant values of the PI controller:

$$K_f(s) = (K_{p,PLL} + \frac{K_{i,PLL}}{s}) + w_e \quad (62)$$

$$K_{i,PLL} = \frac{1}{\tau_{PLL}} \quad (63)$$

$$w_e = 2\pi f_e \quad (64)$$

The complete model of the wind turbine with the VSC can be seen in Figure 3.19.

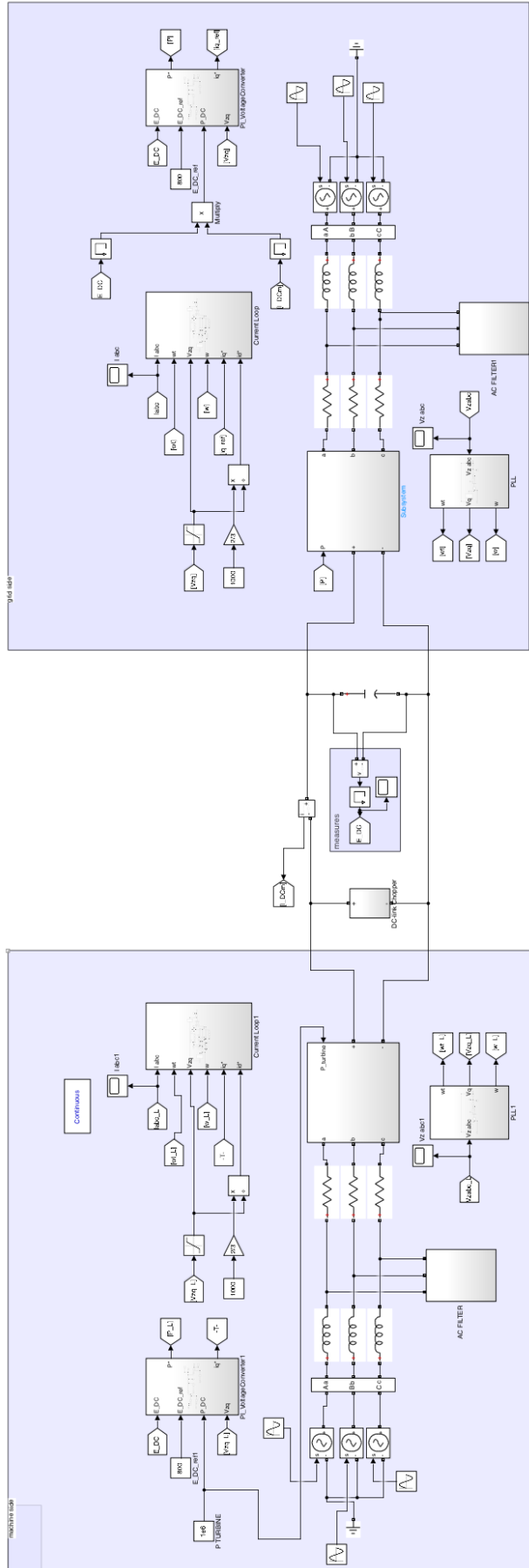


Figure 3.19: VSC complete model with grid side and machine side

Stage	Sub-stage	Period	Control principle	Main parameters
Stage 1	-	t_1-t_3	Ride-through control	k, e_{set}
Stage 2	for P	Stage 2-1	Delay recovery of active power	t_{delay_P}
		Stage 2-2	Ramp recovery of active power	r_p
	for Q	Stage 2-1	Reactive power support	t_{delay_Q}, Q_{supp}
		Stage 2-2	Ramp recovery of reactive power	r_Q

Table 3.1: Different control principles and important parameters at each FRT control stage. [17]

3.4 Fault Ride Through modelling

In this section the full modelling of the Fault Ride Through is presented. In the literature review a brief summary about FRT and different strategies were presented.

The FRT response can be divided in different parts. As seen in Figure 3.20 different recovery waveforms are followed for the reactive power and the active power.

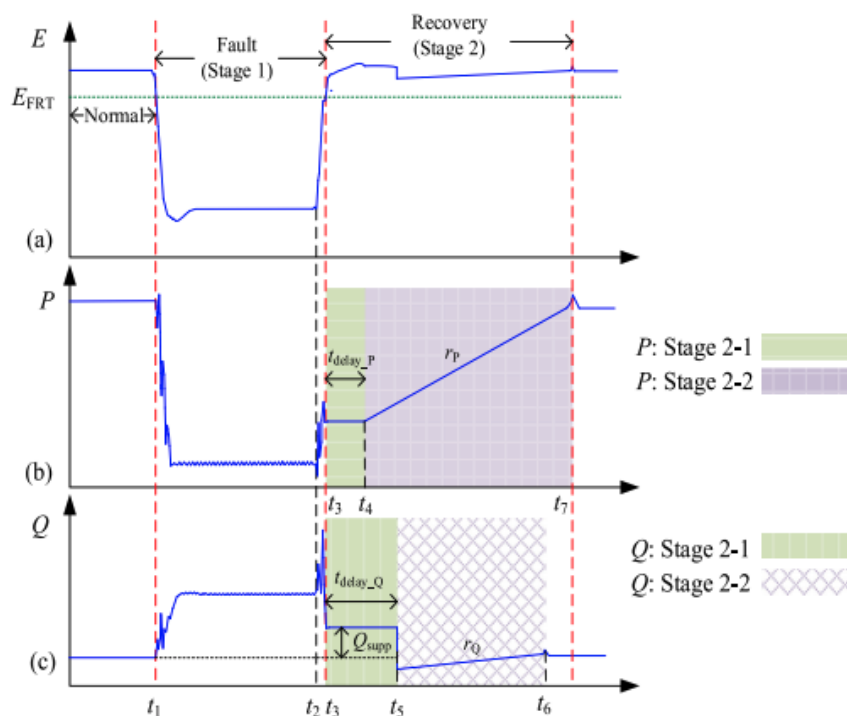


Figure 3.20: Generic FRT response waveforms.[17]

As it can be observed in Figure 3.20 there are different stages during the response which are modelled differently depending if they affect to the active power or to reactive. Table 3.1 summarizes the different stages and the control principle that rides each stage.

If a voltage drop occurs, the WT needs to adjust the output power according to the grid code requirements of the country where is installed.

Figure 3.21 shows a basic scheme of the different control parts to model in the FRT control.

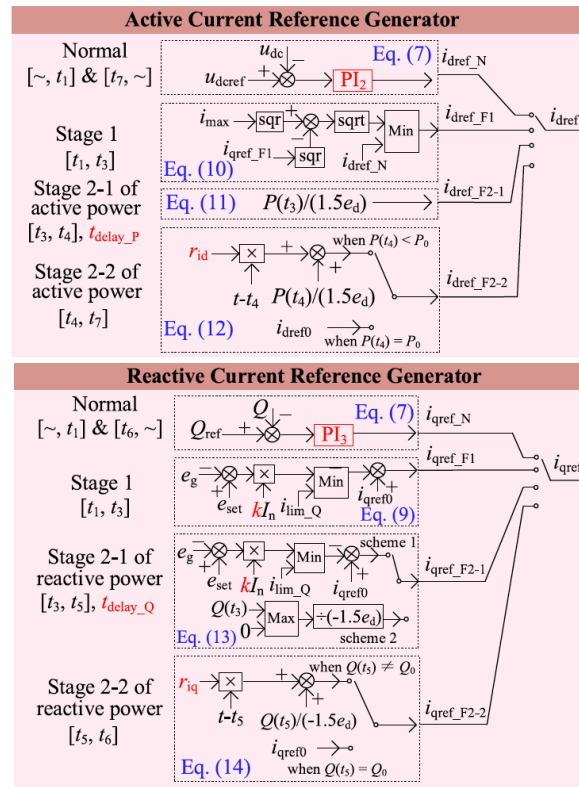


Figure 3.21: Design of active and reactive current reference on the FRT.[17]

On the following pages, the different stages are explained for both active current and reactive current reference, so the turbine can be adapted at each step.

3.4.1 Stage 1: ride-through control during a fault

This stage corresponds to the interval between t_1 and t_3 . The reactive current i_{qref_F1} is given by

$$i_{qref_F1}(t) = -[\min(i_{lim_Q}, k(e_{set} - e_g)l_n)] + i_{qref0} \quad (65)$$

where i_{qref0} is the reactive current reference before the fault. In the case of the active current, i_{dref_F1} is expressed by

$$i_{dref_F1}(t) = (\min(i_{dref_N}, \sqrt{i_{max}^2 - i_{qref_F1}^2})) = \min[(k_{Pudc}(u_{dref} - u_{dc}) + k_{ludc} \int (u_{dref} - u_{dc}) dt, \sqrt{i_{max}^2 - i_{qref_F1}^2}] \quad (66)$$

3.4.2 Stage 2: Post fault recovery control

This stage occurs between t_3 and t_7 and the voltage approximately return to the prefault value. In this stage the control differs between active power and reactive power:

- **Active current reference:** Based on,

$$P_{F1} = 1.5e_d i_d Q_{F1} = -1.5e_d i_q \quad (67)$$

where e_d is the active power, i_d and i_q the respective active and reactive power. And,

$$P_{F2-1}(t) = P(t_3) \quad (68)$$

where $P(t_3)$ is the active power at t_3 , the active current reference $i_{drefF2-1}$ at Stage 2-1 can be obtained as,

$$i_{dref-F2-1}(t) = P(t_3)/(1.5e_d) \quad (69)$$

At Stage 2-2, the current reference $i_{drefF2-2}$ can be obtained as,

$$i_{dref-F2-2}(t) = \begin{cases} r_{id}(t - t_4) + P(t_4)/(1.5e_d), & \text{when } P(t_4) < P_0 \\ i_{dref0}, & \text{when } P(t_4) = P_0 \end{cases} \quad (70)$$

where r_{id} corresponds to the active current recovery rate and i_{dref0} corresponds to the previous active current reference.

- **Reactive current reference:** Similar to active current reference, the reference current for the reactive reference will be derived differently depending on each sub stage of the post fault recovery control. During Stage 2-1, the WT keeps supplying reactive power, so its value $i_{qrefF2-1}$ can be derived as:

$$i_{qref-F2-1}(t) = \begin{cases} -[\min(i_{limQ}, k(e_{set} - e_g)l_n)], & \text{scheme1} \\ \max(Q(t_3), 0)/(-1.5e_d), & \text{scheme2} \end{cases} \quad (71)$$

In Stage 2-2, the control strategy follows the reactive power outer loop control, so the $i_{qrefF2-2}$ can be expressed as,

$$i_{qref-F2-2}(t) = \begin{cases} r_{iq}(t - t_5) + Q(t_5)/(-1.5e_d), & \text{when } Q(t_5) \neq Q_0 \\ i_{qref0}, & \text{when } Q(t_5) = Q_0 \end{cases} \quad (72)$$

where r_{iq} corresponds to the reactive current recovery rate.

Once that all the necessary equations are presented, there are some parameters that needs to be identified. In the case of the FRT control its important to indentify:

- k , corresponds to the reactive power support coefficient which can be calculated under a small voltage dip as:

$$k = (i_{qM0} - i_{qM})/[I_n x (e_{set} - e_g)] \quad (73)$$

where i_{qM0} corresponds to the reactive current measurement previous to the fault.

- r_{id} , corresponds to the active current recovery rate which can be calculated under severe voltage dips, and it can be calculated as:

$$r_{id} = [i_{dM}(t_7) - i_{dM}(t_4)]/(t_7 - t_4) \quad (74)$$

where $i_{dM}(t_x)$ corresponds to the measured active power at t_x .

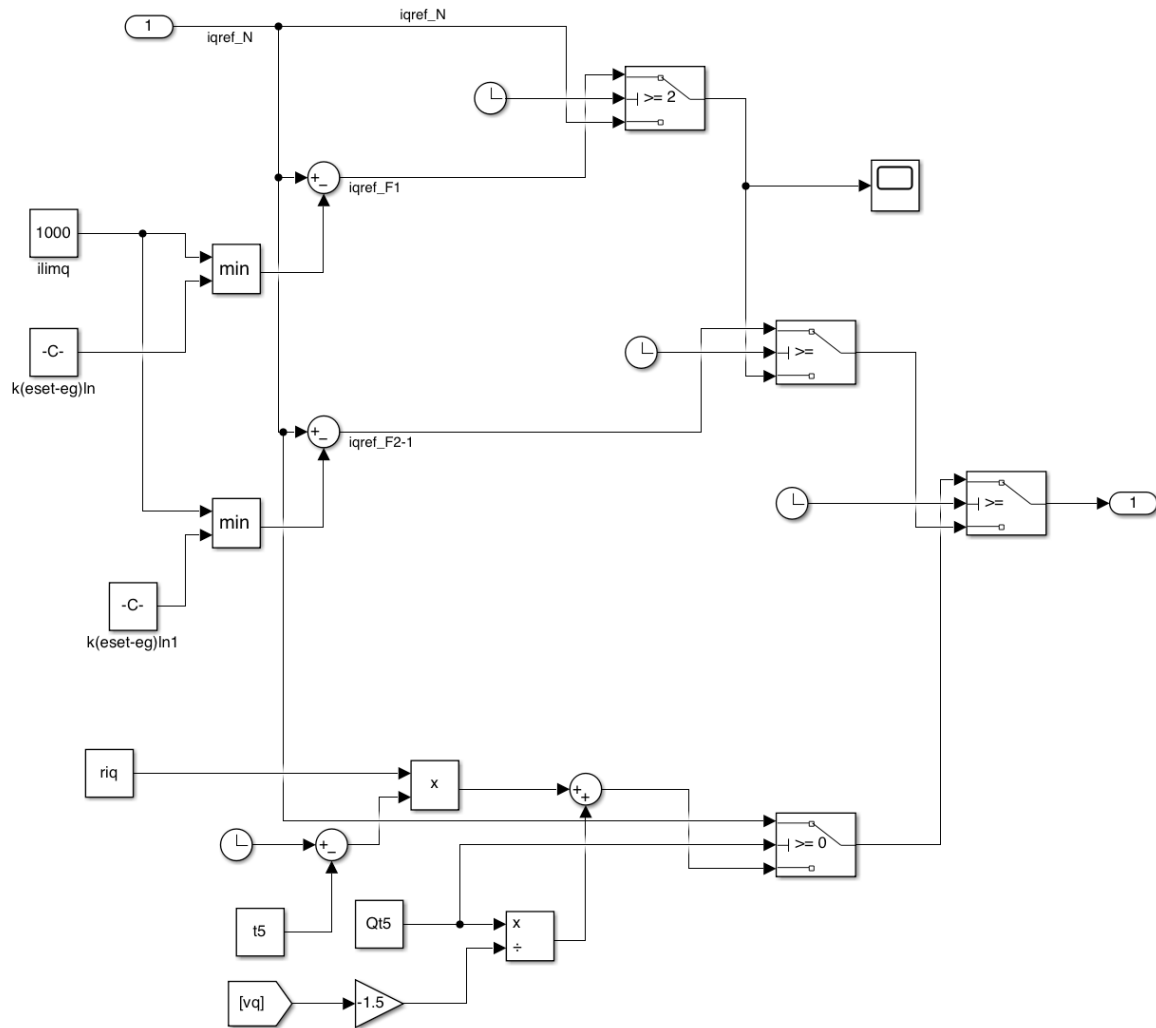


Figure 3.23: Reactive current controller designed in MATLAB.

4 CHAPTER 4: Model validation and results

This section shows simulations carried out to validate the correct design of the WT and its behaviour under a voltage drop.

The chosen wind turbine is a 1.5MW type-4 WT, which has the parameters shown in Table 4.1.

Parameters	Values	Parameters	Values
Rotor diameter	66 m	Generator rated power	1.58 MVA
Cut-in wind speed	3 m/s	Generator rated voltage	0.62 kV
Cut-out wind speed	22 m/s	Generator rated current	1.45 kA
Rated wind speed	12 m/s	Generator frequency	12.69 Hz
DC-link voltage	1.1 kV	Pole pairs	56
Transformer rated capacity	1.6 MVA	Stator resistance	4.35m
Direct-axis inductance	1.6 mH	Quadrature-axis inductance	1.6 mH

Table 4.1: WT parameters for 1.5 MW type-4 WT. [23]

For the design of the VSC the parameters that have been used can be found in Table 4.2. As explained in

Parameters	Controller parameters					
	Current Loop		Voltage controller		PLL	
	k_p	k_i	k_p	k_i	k_p	k_i
Values	5.4	500	0.302	89.48	1	1

Table 4.2: PI parameters for the VSC controller. [21]

the literature review, FRT is guided by the grid code of each country. For this project, the spanish grid code have been used.[24].

The requirements are shown in Figure 4.1 . While the turbine is above the curve, the WT has to stay connected to the grid. In the spanish grid code, turbines has to provide reactive power to support the voltage.

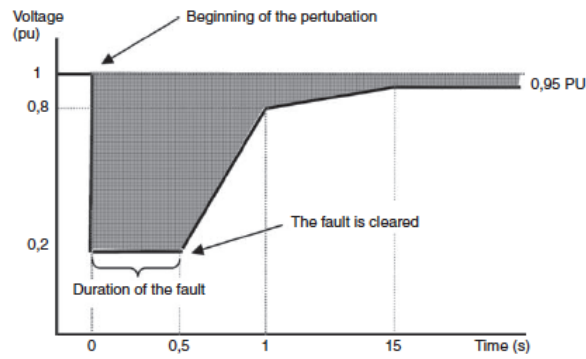


Figure 4.1: Grid code requirements in Spain [25].

Once the different parameters are presented, different simulations can be carried out.

First of all the aerodynamic model is tested to check if it have been modelled correctly. As started in Chapter 3, the power curve can be extracted from the designed code, shown in Appendix A.1.

Using the turbine parameters from [26] as base the following power curve is obtained:

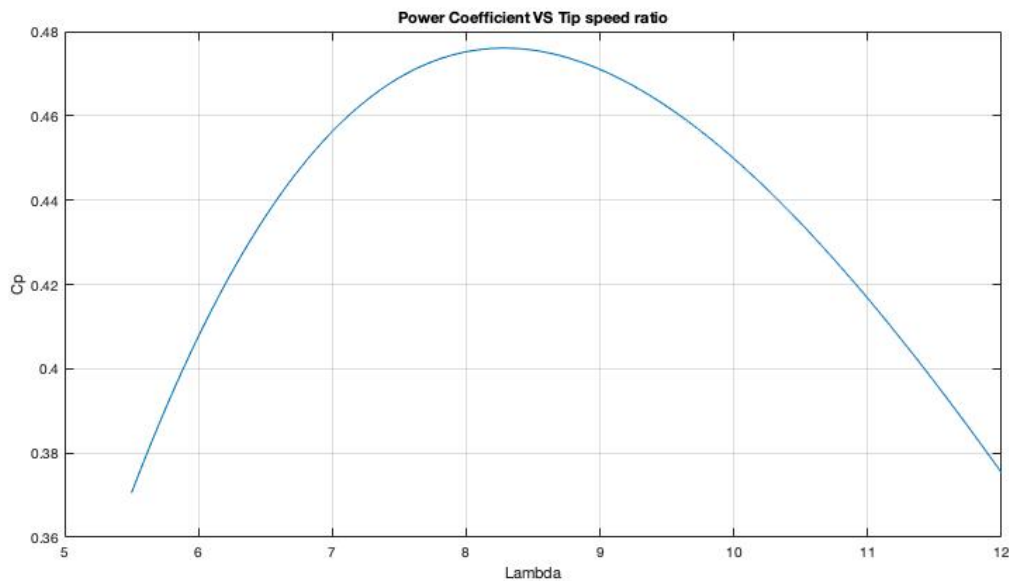


Figure 4.2: C_p curve for the modelled turbine

The obtained curve shows that maximum C_p is almost at 0.475, which corresponds to the value from [26].

The next step is to simulate the PMSG model. The same turbine from [26] is being used which has a nominal torque of $\Gamma_t^N = 0.322e6$ Nm. From the PMSG Matlab model the following curve can be obtained.

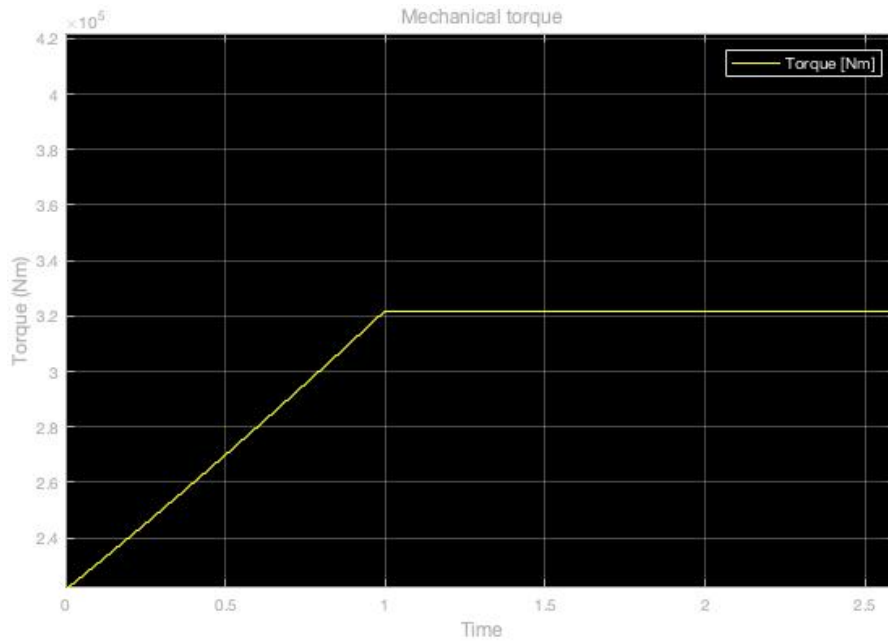


Figure 4.3: Simulated PMSG turbine under nominal conditions.

As Figure 4.3 shows, once the nominal velocity is achieved, the nominal torque is achieved as expected.

One of the objectives of this thesis is to control the turbine in front of changes in the wind speed and parameters of the turbine. This simulations is carried out in order to see how the different parameters of the voltage source converter works and see if the turbine is stabilized and works correctly.

Figure 4.4, shows that as the power generated in the wind turbine changes from 1MW to 1.5MW at $t=1$ s the current i_q is able to stabilize in less than 1s to its current reference value.

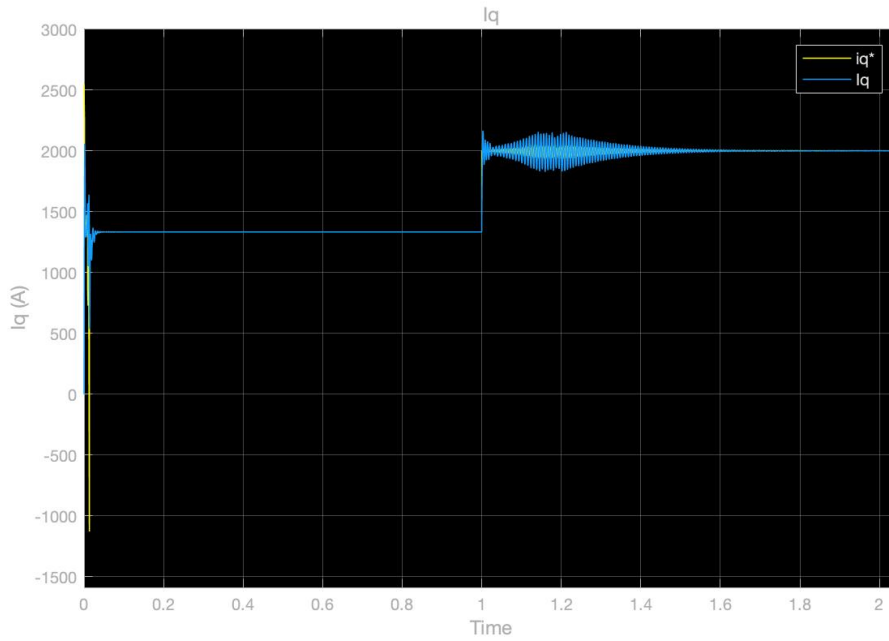


Figure 4.4: i_q simulation for wind speed changes.

Detail of the previous figure is shown in Figure 4.5, where the system tries to return to the 98% of its value after $4\tau_{\text{control-loop}}$, where $\tau_{\text{control-loop}}=0.1\text{s}$. That behaviour shows a good control of the control loop as it is able to stabilize the system with the speed that is requested.

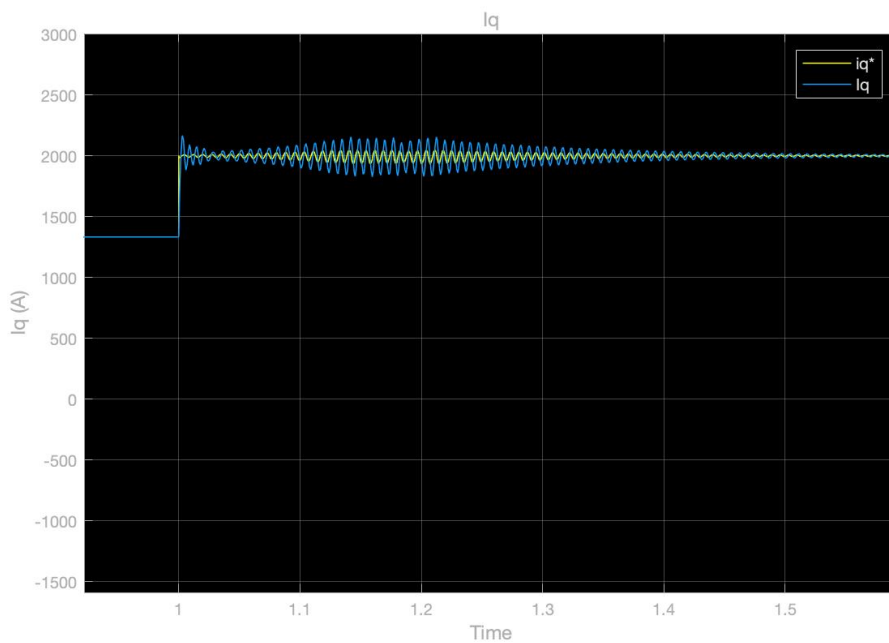


Figure 4.5: i_q detail simulation for wind speed changes.

In the reality, the wind turbine won't suffer this sudden changes in speed so the stabilization will be more smooth, it is true that wind speed changes a lot, but never as a step (what it has been used in order to simulate it).

Following the control principle of the VSC the reactive power is fixed to a desired value [21] and the active power P^* fluctuates in order to regulate the continuous voltage.

For the i_d the following behaviour is obtained as seen in Figure 4.6.

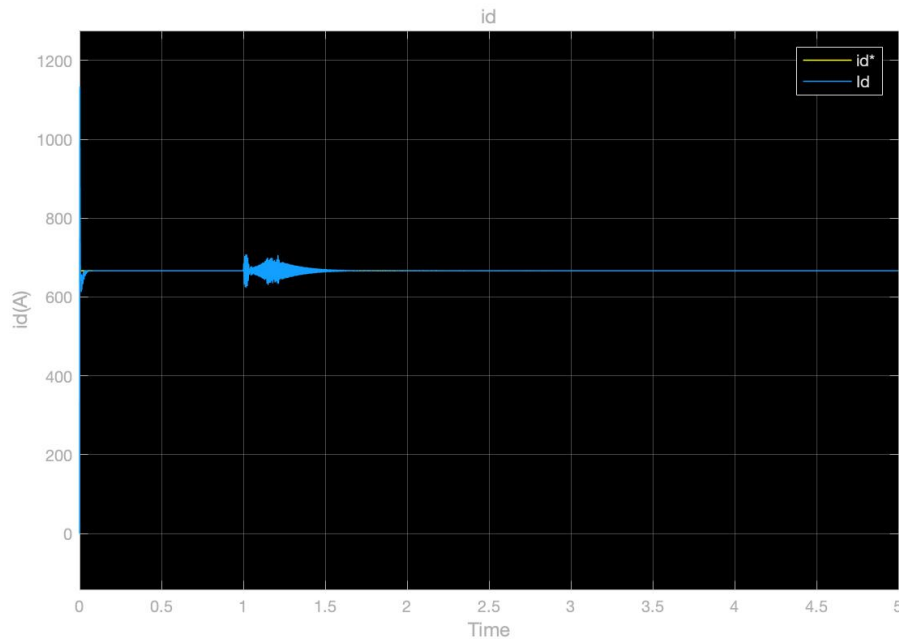


Figure 4.6: i_d simulation for wind speed changes.

The fluctuation on the real value of i_d is due to the changes in the active power, but as the reactive power is constant it returns to the same reference value as before. Figure 4.7 shows the detail of this fluctuation and how in a similar way of i_q it returns to the 98% of its value in $4\tau_{\text{control-loop}}$.

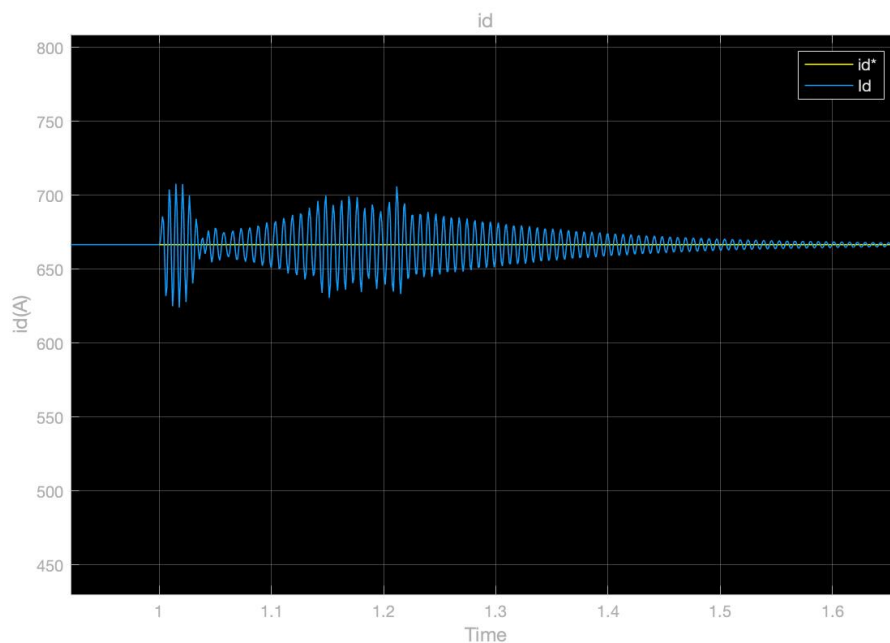


Figure 4.7: i_d detailed simulation for wind speed changes.

The next and final step is to simulate a grid fault and check the behaviour of the full model. For this case, the parameters that have been used are the ones from Table 4.1 and Table 4.2 as solid studies are available to validate the results of this thesis.

This part requires the design of a fault which will be applied to the machine side for the sake of simplicity as seen in Figure 4.8.

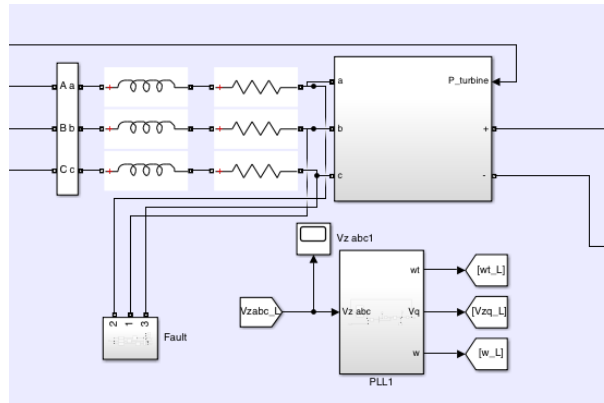


Figure 4.8: Fault implementation to the machine side.

The fault has been implemented as impedance connected to the ground with a switch (Figure 4.9) in order to simulate the fault at specific time.

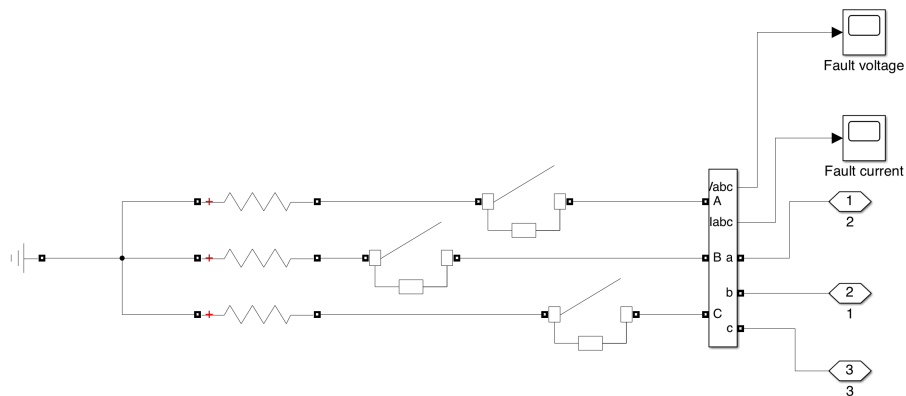


Figure 4.9: Fault detail.

As seen in Figure 4.10 , a fault occurs at $t=2s$ and the current flows through the fault.

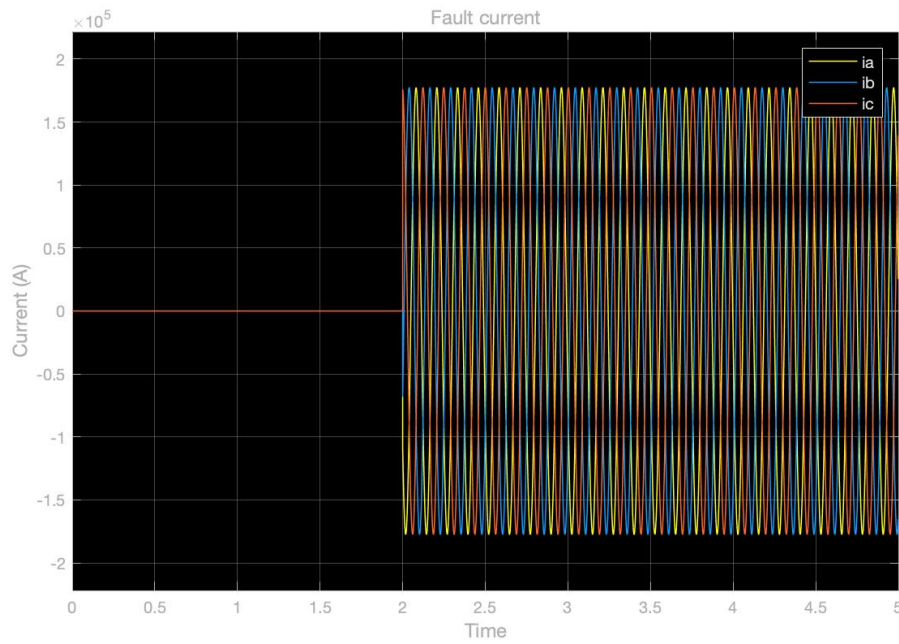


Figure 4.10: Current flow through fault branch.

As exposed in chapter 3, there are different stages on the FRT control methodology, which can be easily a project by itself. As this project focuses in the general modelling and control of the WT, only Stage 1 has been tested and refined, even though all of the different stages have been designed.

Figure 4.11 ,shows that when the fault occurs at $t=2$ s all the current of the machine side is affected.

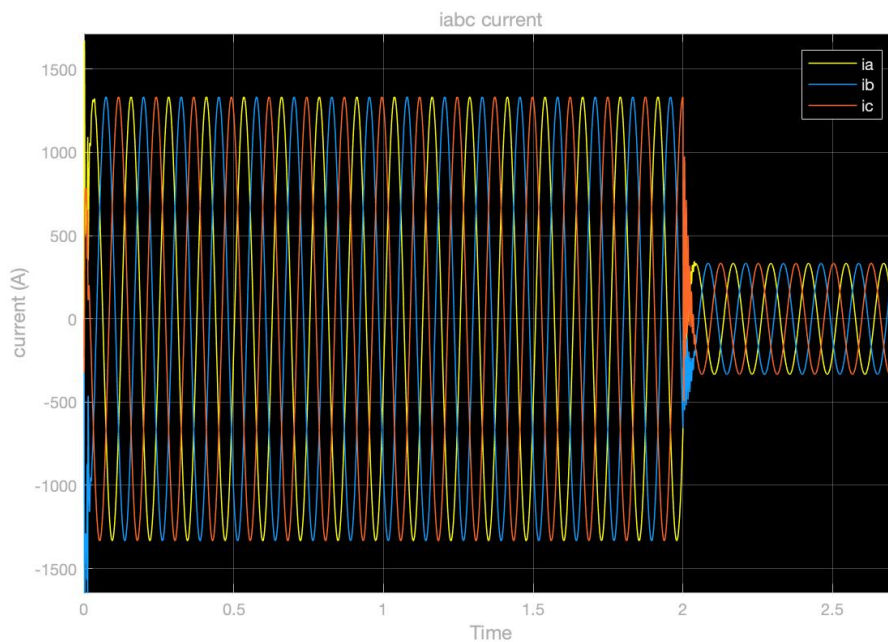


Figure 4.11: MCS current when the fault occurs at $t=2$ s.

Studying in detail the different currents of the converter, it is possible to see that i_q follows the equations

exposed previously of Stage 1, the reactive current adjusts itself as exposed

$$i_{qrefr1}(t) = -[\min(i_{limQ}, k(e_{set} - e_g)l_n)] + i_{qref0} \quad (76)$$

In Figure 4.12, the reactive current decreases and is able to see to its new reference post fault, following the same principle of stabilization than the one exposed for the full VSC modelling.

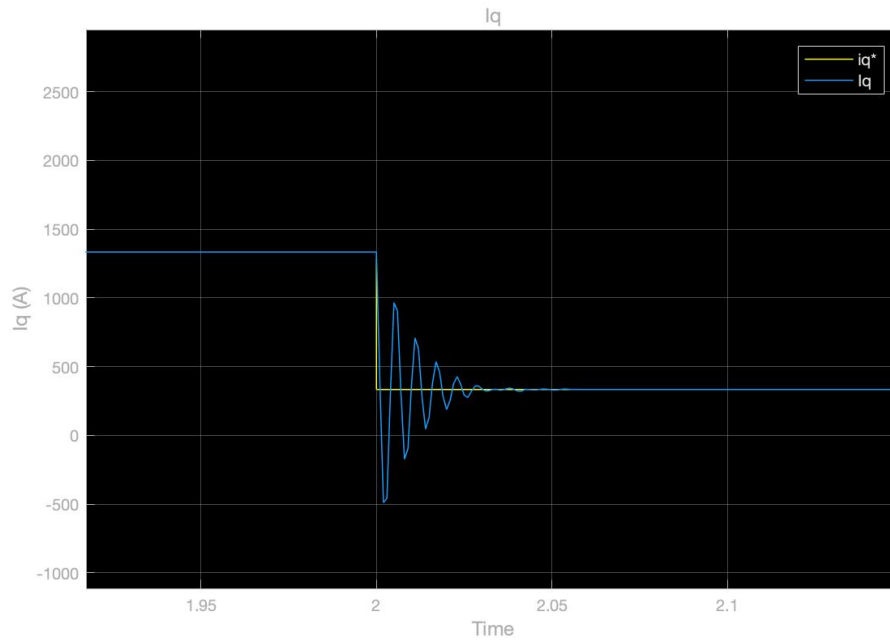


Figure 4.12: Reactive current at t=2s

5 CHAPTER 5: Conclusions and future work

This project covers different topics of the engineering design of a WT, from the aerodynamic part to the dynamic analysis part. The study of the whole system of the turbine has shown that even the most abrupt changes on a WT, which is its normal operation every day, can be overwhelmed with a good control design.

Figure 4.2 has shown that with a good iterative code process is possible to adjust the simulated power curve to the theoretical one given from the literature review. Once that was done, the PMSG model was tested to see if the dynamic model was able to achieve the desired torque and power when wind changes were happening.

Even the changes in wind speed weren't as real as expected, the generator model achieves the expected results as seen in Figure 4.3.

The basic modelling has been able to reproduce quite exactly the theoretical results for the studied wind turbine, as it doesn't require much parameters adjustment.

Once the control part has been tested the results have changed a little. VSC modelling and FRT modelling requires to adjust the different parameters of the PIs of the different control loops.

Full VSC modelling request a lot of design and parameter changes and given the case study has complicated a lot the control. Even that, as seen in Figure 4.4, Figure 4.5, Figure 4.6, Figure 4.7 the controller is able to achieve the reference value of the currents in the requested time for which was designed.

Finally, for the FRT control it was necessary to simplify the scope of the controller as it requires a lot of time to design and test the correct behaviour of it. As some literature explains [28],[29],[30] an iterative process is required to adjust the correct parameters. In order to being able to deliver a decent project in the global scope, this process have been reduced to the post fault control.

As seen in Figure 4.11 and 4.12 the system is able become stable after the fault and not destabilizing. The fault have been applied to the machine side.

5.1 Future work

Following what it was said on the previous section, this project ca be easily enlarge in something more complex. The future work to be done is the following:

- Create an realistic daily wind profile and simulate all the different parts with it.
- For the VSC converter, even it has a good response the parameters can be adjusted in order to get more smooth control
- For the FRT control, the different stages can be adjusted and improved to being able to support all

the fault process.

- As this have been applied to only one offshore WT, the study can be increased to a farm level including different wind turbines with different faults at different times and see how the whole cluster of turbines behaves.
- This study can be a good start for new generation of WT farms as more complex requirements for the grid will be necessary and the integration to the operational grid is an critical part.

A Appendix

A.1 Cp calculation

This code was generated to compute the Cp curve of the selected wind turbine.

```
1 %Simulation of the wind turbine power Output
2 close all , clear all , clc ;
3 %-----
4 %Wind turbine parameters
5 %-----
6 radiu=33;
7 %-----
8 %Efficiency
9 %-----
10 Eff = 0.59;
11 %The density of air at sea level 1.225 kg/m^3
12 %-----
13 densAir=1.225;
14 %-----
15 %Range Vel
16 %-----
17 MinVel=6;
18 MaxVel=14;
19
20 pitch=0;
21 %-----
22 %Define rotor speed from 3/rps to 80 rps
23 %-----
24 MinOmega=1;
25 MaxOmega=80;
26 %-----
27 %
28 %-----
29 Step =0.01;
30 Vel=MinVel : 1 : MaxVel;
31 Omega=MinOmega : Step : MaxOmega;
32 m=length ( Vel ) ;
33 n=length ( Omega ) ;
34 Lmbd=zeros (m, n) ;
```

```

35 %-----
36 %Determine all of Lmbd
37 %-----
38 for i=1:m
39 v=Vel(i);
40 for j=1:n
41 Lmbd(i,j)=radiu*Omega(j)/v;
42 end
43 end
44 %-----
45 %To calculate wind turbines coefficient performance C_p
46 %-----
47 C_p1=1;
48 C_p2=39.52;
49 C_p3=0;
50 C_p4=0;
51 C_p5=0;
52 C_p6=2.04;
53 C_p7=14.47;
54 C_p8=0;
55 C_p9=0;
56 C_p=zeros(m,n);
57 for i=1:m
58 for j=1:n
59 Lamd=Lmbd(i,j);
60 k1=(Lamd+C_p8.*pitch).^(-1)-C_p9/(1+pitch.^3);
61 %C_p(i,j)=C_p1-C_p2*Lamd+C_p3*Lamd^2-C_p4*Lamd^3+C_p5*Lamd^4-C_p6*Lamd^5;
62 C_p(i,j)=max(0,C_p1*(C_p2*k1-C_p3.*pitch-C_p4*pitch.^C_p5-C_p6).*exp(-C_p7*
        k1));
63 if(C_p(i,j)<0)
64 C_p(i,j)=0;
65 end
66 C_p(i,j)=C_p(i,j);
67 end
68 end
69 %-----
70 %
71 %-----
72 Power=zeros(m,n);

```

```

73 for i=1:m
74 v=Vel(i);
75 Power(i,:)=Eff*0.5*C_p(i,:)*densAir*pi*(radiu^2)*(v^3);
76 end
77 %%
78 scrsz = get(0,'ScreenSize');
79 %-----
80 %Plot turbine power vs rotor speed
81 %-----
82 ZeroPos=find(C_p(m,')==0);
83 if (isempty(ZeroPos))
84 Len=n;
85 else
86 Len=ZeroPos-1;
87 end
88 figure('Position',[50 50 scrsz(3)/2-100 scrsz(4)/2-100]);
89 plot(Omega(:,1:Len),Power(:,1:Len));
90 hold on;
91 title('Turbine power versus rotor speed');
92 xlabel('Rotor Speed(rad/s)');
93 ylabel('Power output(w)');
94 %%
95 %-----
96 %Plot turbine maximum power output curve
97 %-----
98 MaxPower=zeros(1,m);
99 Pos=zeros(1,m);
100 MaxValue=1e-6;
101 J=0;
102 for i=1:m
103 MaxPower(i)=max(Power(i,:));
104 MaxValue=max(Power(i,:));
105 J=find(Power(i,')==MaxValue);
106 Pos(i)=J*Step+MinOmega;
107 end
108 plot(Pos,MaxPower,'--.r');
109 hold off;
110 %%
111 %-----

```

```

112 %Label marks for every curve
113 %-----
114 str1='V=';
115 str3=' m/sec ';
116 for i=1:m/2
117 str2=num2str(i+3+0.5);
118 str=strcat(str1, str2);
119 text(Pos((i-1)*2+1),MaxPower((i-1)*2+1), str);
120 str2=num2str(i+3+1);
121 str=strcat(str1, str2);
122 text(Pos(i*2),MaxPower(i*2), str);
123 end
124 %%
125 %-----
126 %Cp vs TSR
127 %-----
128 ZeroPos=find(C_p(1,:) ==0);
129 if(isempty(ZeroPos))
130 Len=n;
131 else
132 Len=ZeroPos-1;
133 end
134 figure('Pos',[scrsz(3)/2 50 scrsz(3)/2-100 scrsz(4)/2-100]);
135 plot(Lmbd(1,1:Len),C_p(1,1:Len));
136 xlim([5,12]);
137 title('Power Coefficient VS Tip speed ratio');
138 xlabel('Lambda');
139 ylabel('Cp');
140 grid on;
141 %%

```

A.2 Model Variables

The following code includes the model variables that are uploaded to the different Simulink files used in the simulation.

```

1 %% TURBINE VARIABLES USED IN THE SIMULINK MODEL
2 % This work is part of the final thesis made by
3 % Joan Francesc Quetglas in IST in collaboration with
4 % CITCEA (UPC)

```

```
5
6
7 %% -----
8 % Simulation time
9 Ts = 5e-06; %seconds
10 T = 1e-4;
11
12 % CHINESE GRID CODE REQUIREMENTS
13 t_fault = 2; %fault starts at t=2
14 t1 = t_fault;
15 t2 = 0.625 + t_fault; %s
16 t3 = 0.7 + t_fault; %s
17 t4 = 0.95 + t_fault;
18 t5 = 1.25 + t_fault;
19 t6 = 2.2 + t_fault;
20 t7 = 2.3 + t_fault;
21
22 Qt5 = 0;
23 Q0 = 0;
24 eg= 0.2; %voltage drop in p.u.
25 k=1.5; %reactive power support coefficient
26 rid = 0.769; %active current recovery rate
27 riq = 0.5; %reactive current recovery rate
28
29
30 eset = 800; %V
31 % Turbine parameters
32 Rt = 31.5; %m
33 U = 12; %m/s
34 wr = 21.57; %rpm
35 pitch = 0; %degrees
36 In = 1470 ; %rated current in A
37 P0 = 1.5e6; %rated power
38
39 % Climate conditions
40
41 phi = 1.225; %density (kg/m3)
42 %% -----
43 %Generator parameters
```

```
44 Ld = 1.6e-3; %Inductances (H)
45 Lq = 1.6e-3;
46
47 Flux = 1.46; %Flux linkage
48 p = 56; %n of pols
49
50 Tf = 0; %static friction
51 R = 0.006; %stator resistance (Ohm)
52 J = 35000; %inertia (kg*m^2)
53
54 Fnom = 60; %Rated frequency (Hz)
55
56 % Initial conditions
57
58 wm = 2*pi*Fnom/p; %rad/s
59 thetam = 0; %degrees
```

A.3 Simulink designs

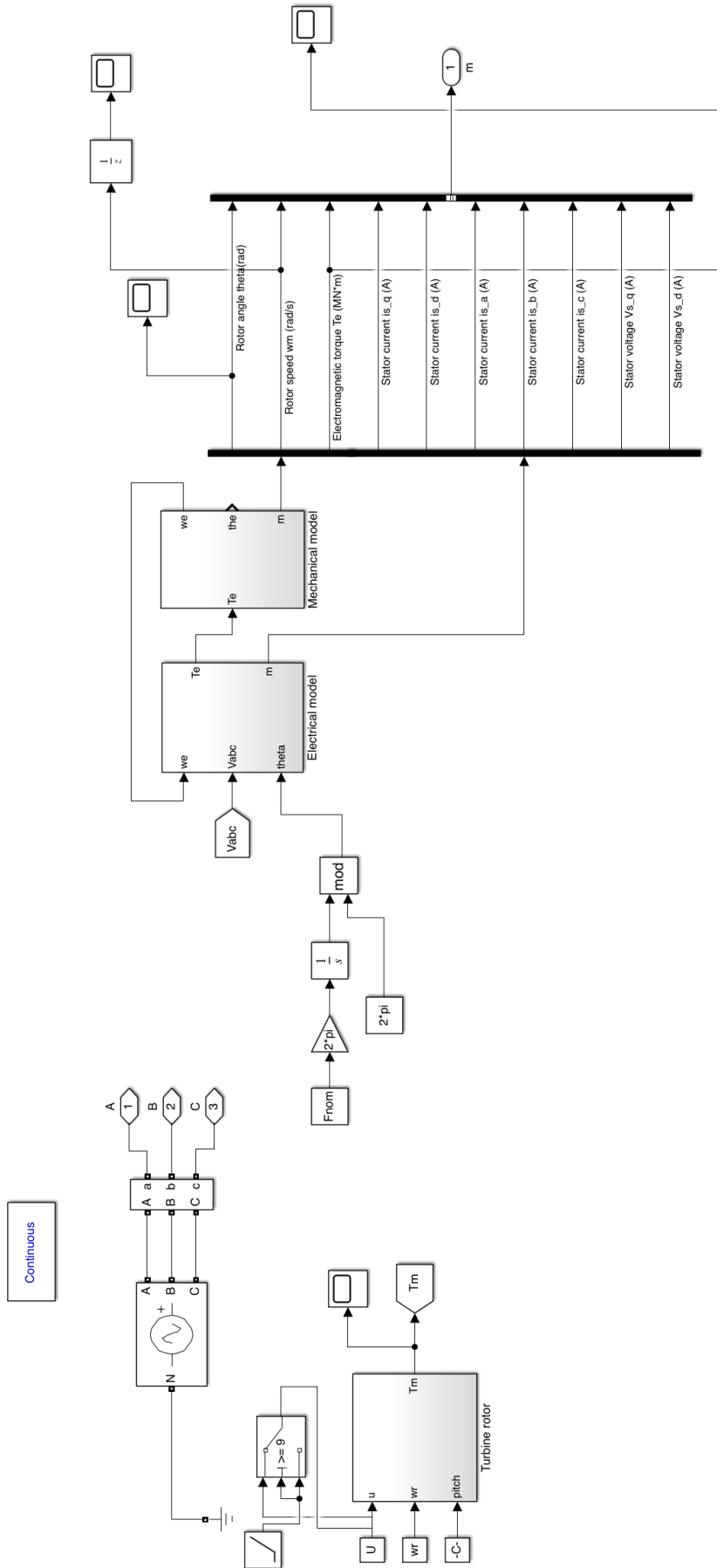


Figure A.1: Full PMSG MODEL

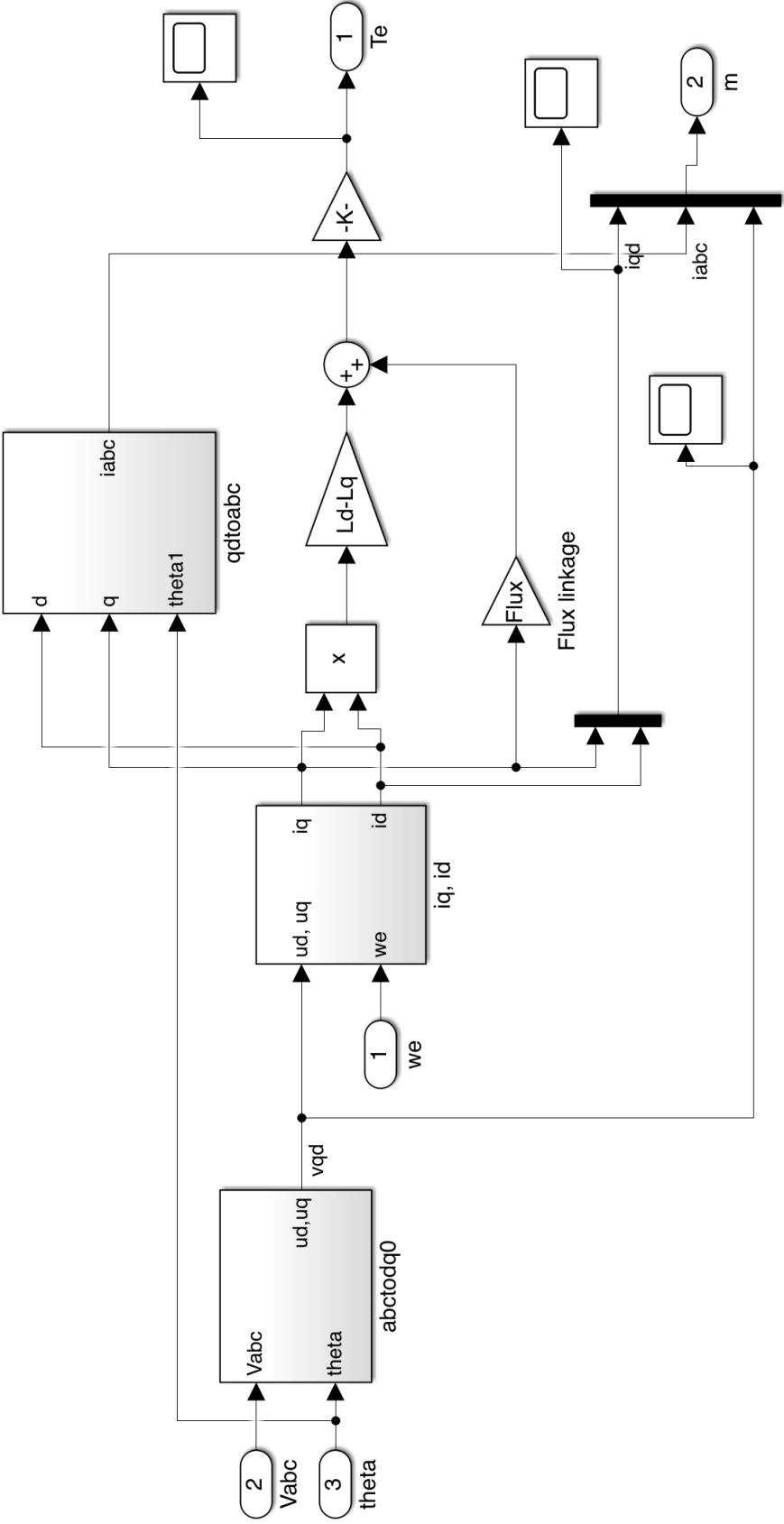


Figure A.3: Electromagnetic torque calculations

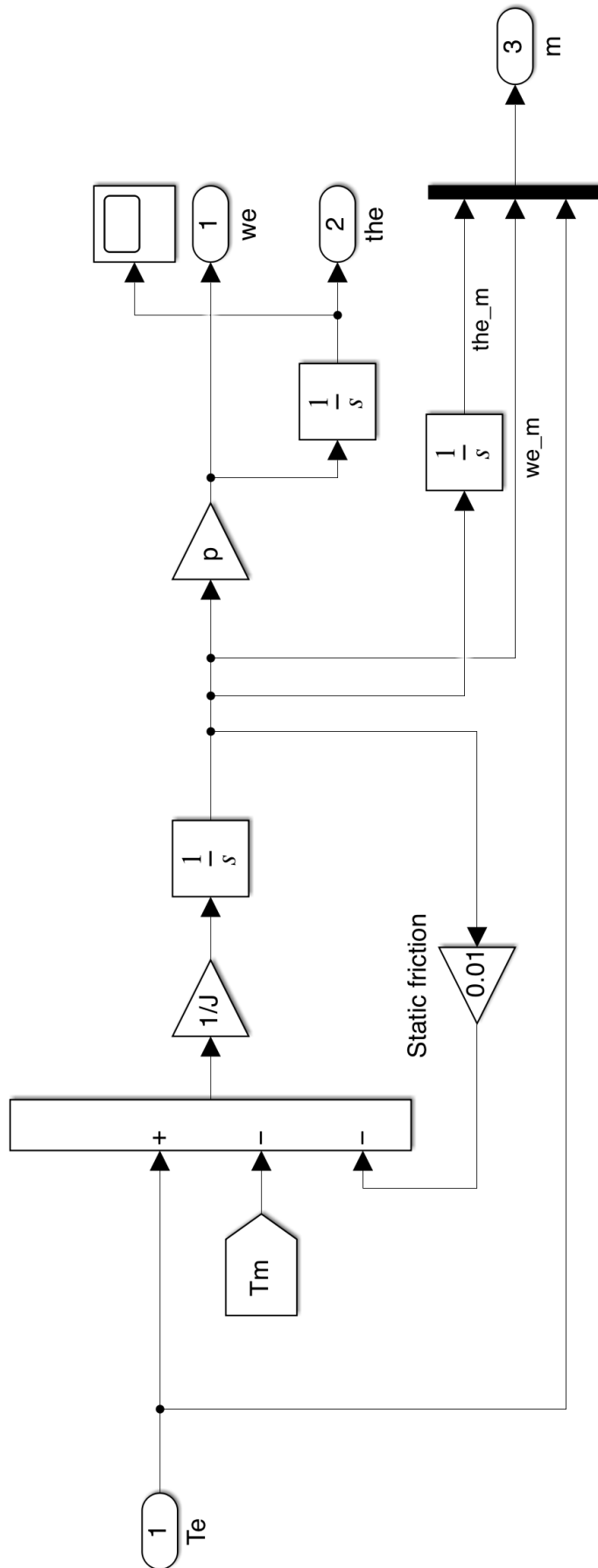


Figure A.4: Torque calculations

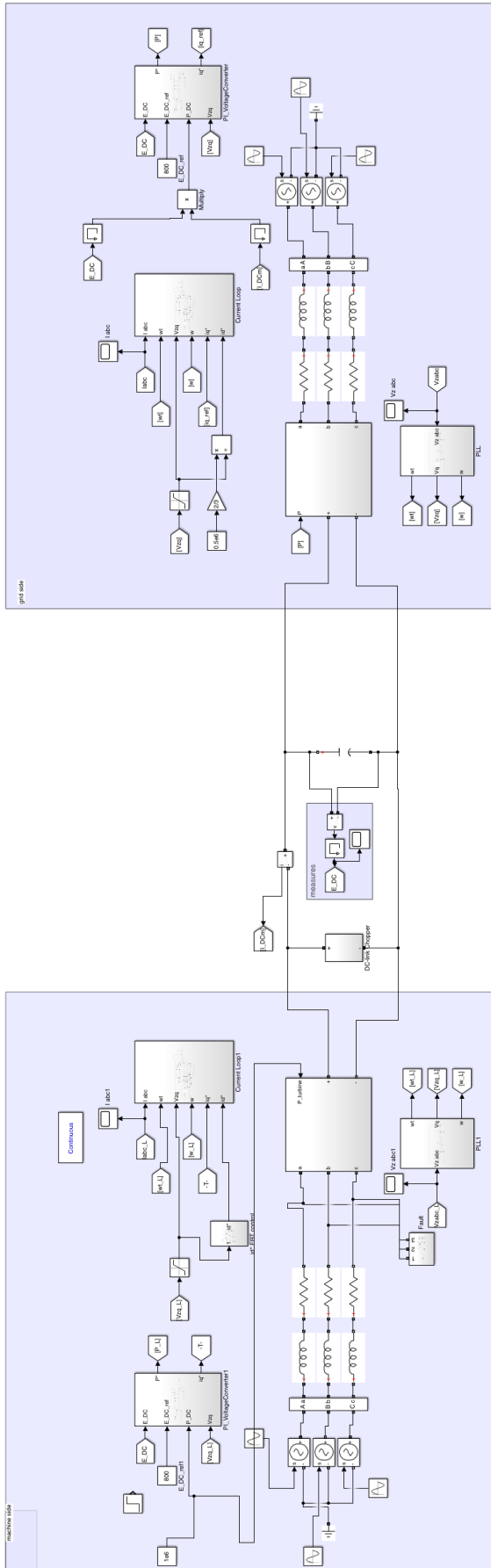


Figure A.5: Full model

Bibliography

- [1] "GLOBAL OFFSHORE WIND REPORT 2020." [ONLINE]. AVAILABLE: WWW.GWEC.NET
- [2] "THE LARGEST OFFSHORE WIND FARM ON THE PLANET OPENS BY AMMAR FRANGOUL." [ONLINE]. AVAILABLE: WWW.CNBC.COM
- [3] "OFFSHORE WIND IN EUROPE." [ONLINE]. AVAILABLE: WWW.WINDEUROPE.ORG
- [4] "RENEWABLE ENERGY STATISTICS 2021," [ONLINE]. AVAILABLE: WWW.IRENA.ORG
- [5] G. VENKATARAMANAN AND C. MARNAY, "A LARGER ROLE FOR MICROGRIDS," *IEEE POWER AND ENERGY MAGAZINE*, VOL. 6, NO. 3, 2008, DOI: 10.1109/MPE.2008.918720.
- [6] B. KROPOSKI, R. LASSETER, T. ISE, S. MOROZUMI, S. PAPATHANASSIOU, AND N. HATZIARGYRIOU, "MAKING MICROGRIDS WORK," *IEEE POWER AND ENERGY MAGAZINE*, VOL. 6, NO. 3, 2008, DOI: 10.1109/MPE.2008.918718.
- [7] A. D. HANSEN ET AL., "MAPPING OF GRID FAULTS AND GRID CODES - RISØ-R-1617(EN)," *IEEE TRANSACTIONS ON ENERGY CONVERSION*, VOL. 35, NO. 3, 2008.
- [8] I. ERLICH, W. WINTER, AND A. DITTRICH, "ADVANCED GRID REQUIREMENTS FOR THE INTEGRATION OF WIND TURBINES INTO THE GERMAN TRANSMISSION SYSTEM," 2006. DOI: 10.1109/PES.2006.1709340.
- [9] T. ACKERMANN, "WIND POWER IN POWER SYSTEMS". ROYAL INSTITUTE OF TECHNOLOGY, 2005. DOI: 10.1002/0470012684.
- [10] V. DAHIYA AND L. G., "COMPARATIVE STUDY OF DOUBLY FED INDUCTION GENERATOR AND PERMANENT MAGNET SYNCHRONOUS GENERATOR IN WIND ENERGY CONVERSION SYSTEM," *INTERNATIONAL JOURNAL OF ELECTRICAL ENGINEERING TECHNOLOGY*, VOL. 10, NO. 3, 2019, DOI: 10.34218/IJEET.10.3.2019.009.
- [11] M. NASIRI AND R. MOHAMMADI, "PEAK CURRENT LIMITATION FOR GRID SIDE INVERTER BY LIMITED ACTIVE POWER IN PMSG-BASED WIND TURBINES DURING DIFFERENT GRID FAULTS," *IEEE TRANS SUSTAIN ENERGY*, VOL. 8, NO. 1, 2017, DOI: 10.1109/TSTE.2016.2578042.
- [12] D. M. YEHIA, D. E. A. MANSOUR, AND W. YUAN, "FAULT RIDE-THROUGH ENHANCEMENT OF PMSG WIND TURBINES WITH DC MICROGRIDS USING RESISTIVE-TYPE SFCL," *IEEE TRANSACTIONS ON APPLIED SUPERCONDUCTIVITY*, VOL. 28, NO. 4, 2018, DOI: 10.1109/TASC.2018.2821362.
- [13] M. NASIRI, J. MILIMONFARED, AND S. H. FATHI, "A REVIEW OF LOW-VOLTAGE RIDE-THROUGH ENHANCEMENT METHODS FOR PERMANENT MAGNET SYNCHRONOUS GENERATOR BASED WIND TURBINES," *RENEWABLE AND SUSTAINABLE ENERGY REVIEWS*, VOL. 47. 2015. DOI: 10.1016/j.rser.2015.03.079.

- [14] J. F. CONROY AND R. WATSON, "LOW-VOLTAGE RIDE-THROUGH OF A FULL CONVERTER WIND TURBINE WITH PERMANENT MAGNET GENERATOR," *IET RENEWABLE POWER GENERATION*, VOL. 1, NO. 3, 2007, DOI: 10.1049/IET-RPG:20070033.
- [15] A. GENCER, "ANALYSIS AND CONTROL OF FAULT RIDE THROUGH CAPABILITY IMPROVEMENT PMSG BASED ON WECS USING ACTIVE CROWBAR SYSTEM DURING DIFFERENT FAULT CONDITIONS," *ELEKTRONIKA IR ELEKTROTEHNIKA*, VOL. 24, NO. 2, 2018, DOI: 10.5755/J01.EIE.24.2.20637.
- [16] M. R. ISLAM ET AL., "FAULT RIDE THROUGH CAPABILITY IMPROVEMENT OF DFIG BASED WIND FARM USING NON-LINEAR CONTROLLER BASED BRIDGE-TYPE FLUX COUPLING NON-SUPERCONDUCTING FAULT CURRENT LIMITER," *ENERGIES (BASEL)*, VOL. 13, NO. 7, 2020, DOI: 10.3390/EN13071696.
- [17] K. E. OKEDU, "IMPROVING THE PERFORMANCE OF PMSG WIND TURBINES DURING GRID FAULT CONSIDERING DIFFERENT STRATEGIES OF FAULT CURRENT LIMITERS," *FRONT ENERGY RES*, VOL. 10, JUN. 2022, DOI: 10.3389/FENRG.2022.909044.
- [18] K. E. OKEDU, "EFFECT OF ECS LOW-PASS FILTER TIMING ON GRID FREQUENCY DYNAMICS OF A POWER NETWORK CONSIDERING WIND ENERGY PENETRATION," IN *IET RENEWABLE POWER GENERATION*, 2017, VOL. 11, NO. 9. DOI: 10.1049/IET-RPG.2016.0855.
- [19] J. HASAN, M. R. ISLAM, M. R. ISLAM, A. Z. KOUZANI, AND M. A. P. MAHMUD, "A CAPACITIVE BRIDGE-TYPE SUPERCONDUCTING FAULT CURRENT LIMITER TO IMPROVE THE TRANSIENT PERFORMANCE OF DFIG/PV/SG-BASED HYBRID POWER SYSTEM," *IEEE TRANSACTIONS ON APPLIED SUPERCONDUCTIVITY*, VOL. 31, NO. 8, 2021, DOI: 10.1109/TASC.2021.3094422.
- [20] B. MOHAMED EBEED HUSSEIN AL-KHARBOSY AND P. ABDULLA AHMED EBRAHIM OMAR NOURELDEEN SOLIMAN, "ENHANCEMENT PROTECTION AND OPERATION OF THE DOUBLY FED INDUCTION GENERATOR DURING GRID FAULT," 2012, DOI:10.13140/RG.2.2.16718.25925
- [21] A. EGEA-ALVAREZ, A. JUNYENT-FERRÉ, AND O. GOMIS-BELLMUNT, "ACTIVE AND REACTIVE POWER CONTROL OF GRID CONNECTED DISTRIBUTED GENERATION SYSTEMS," *GREEN ENERGY AND TECHNOLOGY*, VOL. 96, 2012, DOI: 10.1007/978-3-642-22904-63.
- [22] J. Qi, W. Li, P. Chao, X. Liang, Y. Sun, and Z. Li, "Generic EMT modeling method of Type-4 wind turbine generators based on detailed FRT studies," *Renew Energy*, vol. 178, 2021, doi: 10.1016/j.renene.2021.06.057.
- [23] J. G. SLOOTWEG AND W. L. KLING, "MODELLING WIND TURBINES FOR POWER SYSTEM DYNAMICS SIMULATIONS: AN OVERVIEW," *WIND ENGINEERING*, VOL. 28, NO. 1 SPEC. ISS. 2004. DOI: 10.1260/0309524041210801.
- [24] YUANZHANG SUN, "MODELING AND MODERN CONTROL OF WIND POWER". WILEY-IEEE PRESS, 2018. DOI: 10.1002/9781119236382

- [25] MINISTERIO DE INDUSTRIA DE ESPAÑA, "PO 12.3. REQUISITOS DE RESPUESTA FRENTE A HUECOS DE TENSIÓN DE LAS INSTALACIONES EÓLICAS," *BOE*, VOL. 254, 2006.
- [26] A. JUNYENT-FERRÉ, "CONTROL OF POWER ELECTRONIC CONVERTERS FOR THE OPERATION OF WIND GENERATION SYSTEMS UNDER GRID DISTURBANCES," DOCTORAL THESIS, UPC, DEPARTMENT OF ELECTRICAL ENGINEERING, 2011. [ONLINE]. AVAILABLE: [HTTP://HDL.HANDLE.NET/2117/94751](http://hdl.handle.net/2117/94751)
- [27] T. M. SOBY, M. WAHAB, N. G. A. HEMDAN, M. M. HAMADA, AND M. A. A. WAHAB, "GERMAN GRID CODE ASPECTS DISCUSSION: LOW VOLTAGE RIDE-THROUGH OF CONVERTER BASED DECENTRALIZED GENERATION REACTIVE POWER MANAGEMENT IN DISTRIBUTION NETWORKS VIEW PROJECT GERMAN GRID CODE ASPECTS DISCUSSION: LOW VOLTAGE RIDE-THROUGH OF CONVERTER BASED DECENTRALIZED GENERATION." [ONLINE]. AVAILABLE: [HTTPS://WWW.RESEARCHGATE.NET/PUBLICATION/281109399](https://www.researchgate.net/publication/281109399)
- [28] J. QI, W. LI, P. CHAO, X. LIANG, Y. SUN, AND Z. LI, "GENERIC EMT MODELING METHOD OF TYPE-4 WIND TURBINE GENERATORS BASED ON DETAILED FRT STUDIES," *RENEW ENERGY*, VOL. 178, 2021, DOI: 10.1016/j.renene.2021.06.057.
- [29] A. GENCER, "ANALYSIS AND CONTROL OF FAULT RIDE-THROUGH CAPABILITY IMPROVEMENT FOR WIND TURBINE BASED ON A PERMANENT MAGNET SYNCHRONOUS GENERATOR USING AN INTERVAL TYPE-2 FUZZY LOGIC SYSTEM," *ENERGIES (BASEL)*, VOL. 12, NO. 12, 2019, DOI: 10.3390/en12122289
- [30] X. YAN, L. YANG, AND T. LI, "THE LVRT CONTROL SCHEME FOR PMSG-BASED WIND TURBINE GENERATOR BASED ON THE COORDINATED CONTROL OF ROTOR OVERSPEED AND SUPERCAPACITOR ENERGY STORAGE," *ENERGIES (BASEL)*, VOL. 14, NO. 2, JAN. 2021, DOI: 10.3390/en14020518.E